Development of an Active Flight Envelope Warning Method for General Aviation Aircraft

An Undergraduate Honors Thesis

Presented in partial fulfillment of the requirements for graduation with Honors Research Distinction in the College of Engineering at The Ohio State University

By

Steven R. Scherer

Thesis Committee:

Dr. Clifford A. Whitfield, Advisor

Dr. Richard J. Freuler

Matthew McCrink

The Ohio State University

Department of Mechanical and Aerospace Engineering

May 2015

Abstract

The term "general aviation" accounts for all civilian flights that are not scheduled (or chartered) passenger airlines. Loss of control incidents in flight are the primary cause of fatal general aviation accidents. By definition, a loss of control event is a preventable occurrence where a pilot should have maintained or regained control of their aircraft. Giving a pilot sufficient warning to correct dangerous situations is crucial in preventing loss of control. Existing warning methods are based on physical margins of aircraft limitations and do not directly consider how much time is left to act before loss of control. This research focuses on the development of a method that uses real-time inertial and aerodynamic data to calculate and improve warnings of flight envelope limitations. X-Plane 10, a realistic flight simulator, was used to simulate the flight of a Cessna 172, a common general aviation aircraft. The flight model of X-Plane has been compared to empirical data with favorable results, indicating X-Plane is a reasonable platform on which to investigate an active warning system. The development of an X-Plane software plugin for a constant-time warning system method is discussed in detail. The plugin utilizes aircraft and flight model data from X-Plane to consider proximity to a potential loss of control event before issuing a warning. When configured to warn the pilot 2.2 seconds before loss of control, coefficient of lift based methods showed up to an additional 1.1 seconds of margin when compared to traditional stall warning methods and an overall stall warning margin of approximately 2 seconds. With careful consideration

of the physical state of the aircraft, the system is meant to give the pilot at least 2 or 3 seconds to correctly react to a dangerous situation. This type of "constant-time" warning is a novel approach to preventing loss of control and offers distinct advantages over more traditional methods, which can leave pilots with very little time to react. The method demonstrated can use visual and aural warnings and can be modified to adjust its time warning margin based on the potential for fatal loss of control. Such a system could be integrated into current general aviation aircraft using digital cockpit hardware or a standalone electronic box. The proof-of-concept created for this warning technique opens possibilities of more capable yet less costly loss of control mitigation systems that have the potential to greatly reduce general aviation fatalities.

Dedication

To my wife and family,
for their unwavering support in the pursuit of my dreams.

To my grandparents,
who enabled and encouraged the flight training that inspired this work.

Acknowledgements

I am forever indebted to and express sincere gratitude toward my advisor, Dr. Whitfield, for all of his time and enthusiasm that helped propel this project to completion. Without such guidance, I would still be chasing down loose ends. I thank him for each and every time he stopped what he was doing to assist in my research.

I am grateful for all of my committee members, Dr. Whitfield, Dr. Freuler, and Matthew McCrink. Your insightful feedback and constructive criticism has improved this document and given me new perspectives on how to present work to others. I appreciate your time and flexibility in working with this research.

To the College of Engineering Honors program for their generous financial support through a research scholarship, thank you. I have thoroughly enjoyed my experience in the Honors program and I am honored to have my research selected as worthy of financial support.

Finally, I would like to express my thanks and gratitude to all of my family and friends who have provided support and feedback throughout this research. I was able to pursue and complete this research because of the positive influences that have been exerted on me over the years.

Table of Contents

List of Figures

List of Tables

List of Symbols and Abbreviations

Acronyms and Abbreviations

AC	aerodynamic center
c.g.	center of gravity
DATCOM	data compendium (United States Air Force calculation methods)
EFIS	electronic flight instrument system
FAA	Federal Aviation Administration
FAR	Federal Aviation Regulation
FBW	fly-by-wire
GA	general aviation
IMU	inertial measurement unit
KIAS	knots indicated airspeed
LoC	loss of control
MAC	mean aerodynamic chord
MSL	mean sea level (altitude)
NTSB	National Transportation Safety Board
POH	pilot's operating handbook
SA	situational awareness
SDK	software development kit
SLUF	straight, level, unaccelerated flight
w.r.t	with respect to

English Letters

A	aspect ratio
b	span
$\bar{c}$	mean aerodynamic chord
c_r	root chord
c_t	tip chord
e	Oswald's efficiency factor
L	lifting force
L_f	length of fuselage
S	reference area
v	velocity
W_f	width of fuselage

Greek Symbols

α	angle of attack
λ	taper ratio
Λ_{LE}	leading-edge sweep
$\Lambda_{\mathrm{c/4}}$	quarter-chord sweep
$\Lambda_{\mathrm{c/2}}$	semi-chord sweep
Λ_{TE}	trailing-edge sweep
θ	pitch
ϕ	roll
ψ	heading
ρ	air density

Common Subscripts

c/2	half-chord
c/4	quarter-chord
E	elevator
HT	horizontal tail
F	flap
f	fuselage
LE	leading edge
r	root
t	tip
TE	trailing edge
w	wing
WB	wing-body
VT	vertical tail
∞	freestream

Stability Derivatives

C_{ℓ_β}	change in rolling moment coefficient w.r.t angle of sideslip
C_{L_α}	change in lift coefficient w.r.t. angle of attack (lift-curve slope)
$C_{L_{\delta E}}$	change in lift coefficient w.r.t. elevator deflection
$C_{L_{\delta F}}$	change in lift coefficient w.r.t. flap deflection
C_{M_α}	change in pitching moment coefficient w.r.t. angle of attack
$C_{M_{\delta E}}$	change in pitching moment coefficient w.r.t. elevator deflection
$C_{M_{\delta F}}$	change in pitching moment coefficient w.r.t flap deflection
C_{N_β}	change in yawing moment coefficient w.r.t angle of sideslip

Chapter 1: Introduction

1.1 Background

The term "general aviation" (GA) accounts for all civilian flights that are not scheduled (or chartered) passenger airlines. General aviation aircraft tally more than 90% of the registered aircraft in the United States [1]. Agriculture, law enforcement, personal flying, land surveying, medical services, skydiving, and flight training are just a few examples of what falls under general aviation flying. Of all general aviation flights, an estimated 65% are for business and public services [1]. The other third of GA flights are for personal flying, which might include visiting family or friends, flying for pleasure, flying to reach a vacation destination, or flying for proficiency. While personal flying only accounts for one-third of GA flying, it accounts for two-thirds of GA accidents [2].

1.1.1 General Aviation Accidents Overview

More than 65% of accidents in general aviation throughout 2012 occurred during personal flying operations [2]. Table 1 on the following page gives an overview of GA accidents that occurred in 2012. The numbers are broken down by the purpose of flight. For the complete table, see Table A-1 in Appendix A.

While personal flying only accounts for about one-third of all GA flights, approximately 73% of GA fatalities from 2003-2012 occurred during personal use [2].

For this reason, the focus of the present research is turned toward safety of personal flying in general aviation.

Table 1: General aviation accidents from 2012 NTSB data [2]

General Aviation Accident Aircraft by Flight Purpose, 2012		
Purpose of Flight	**Total Accidents**	**Percent of Total**
Personal	988	66.40%
Instructional	208	14.00%
Aerial Application	67	4.50%
Business	31	2.10%
All Other	193	13.00%
Total	**1487**	**100%**

Figure 1 below indicates a decline in personal flying hours over the past decade. The exact cause of this decline, while beyond the scope of this work, might be attributed to increasing costs of flying or perhaps the declining pilot population.

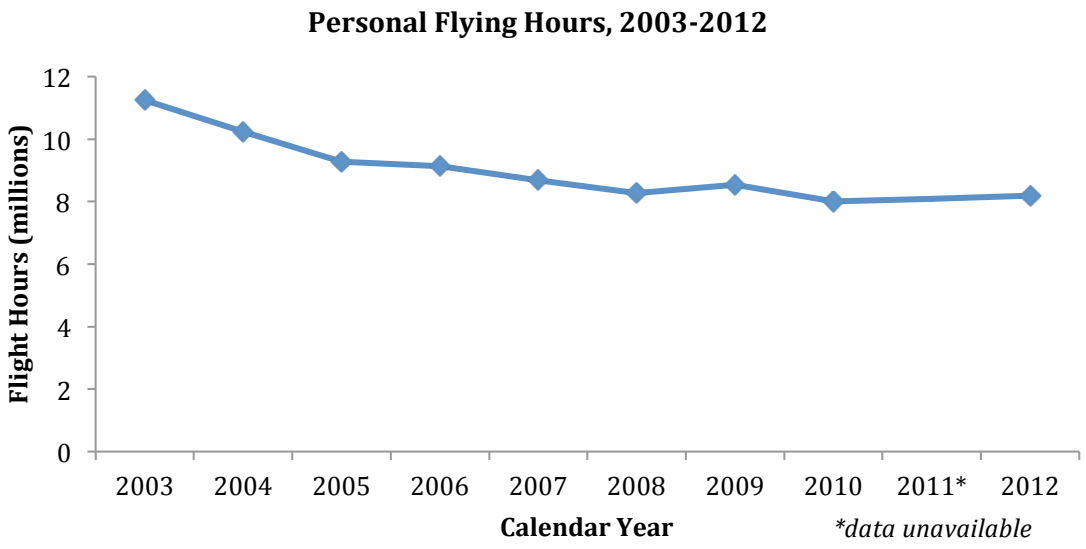

Figure 1: Personal flying hours data from 2012 analysis [2]

While there is no denying that personal flying hours have gone down in the past decade, Figure 2 on the following page makes it clear that the accident rate has actually stayed relatively stagnant or even slightly increased over the same period.

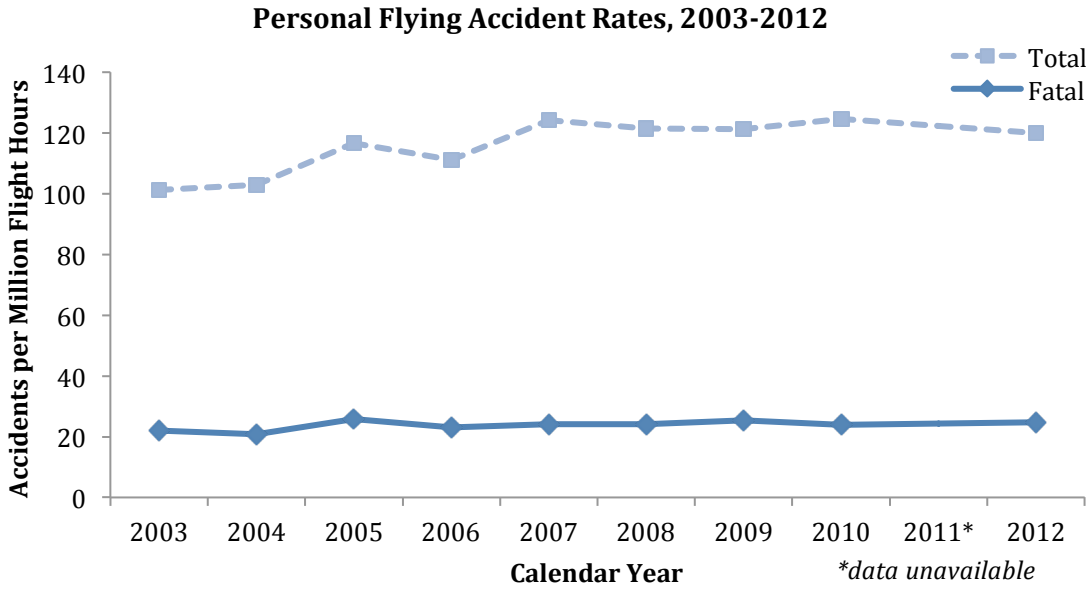

Figure 2: Personal flying accident rates, 2003-2012 [2]

With stagnant accident rates in personal flying, it is important to understand what is causing so many accidents and their resulting fatalities.

1.1.2 Loss of Control Events: Definition and Statistics

Loss of control inflight (LoC) generally occurs when an aircraft enters a flight condition that exceeds the normal realm of flight operations, known as the flight envelope. According to Rich Stowell (MCFI-A), LoC accidents result from "situations in which a pilot should have maintained or regained control of the aircraft, but did not" [3]. Cockpit distractions, lack of situational awareness, or mishandling of the aircraft can contribute to an LoC event. In these situations, inappropriate (or lack of) flight control inputs can quickly result in a deadly stall or spin. LoC incidents are the primary cause of fatal general aviation accidents [2].

Figure 3 on the following page presents data derived from a 2012 National Transportation Safety Board (NTSB) report about general aviation accidents in personal

flying. During an accident investigation, the NTSB attempts to identify a defining event (or primary cause) of the accident. The number of accidents for a defining event, both fatal and non-fatal, is organized in descending order of frequency. As shown for calendar year 2012, LoC inflight situations accounted for 20% of all accidents. Out of 203 fatal GA personal flying accidents in 2012, 92 (45%) were primarily caused by Loss of Control inflight [2]. For the complete list of defining events, see Figure A-1 in Appendix A.

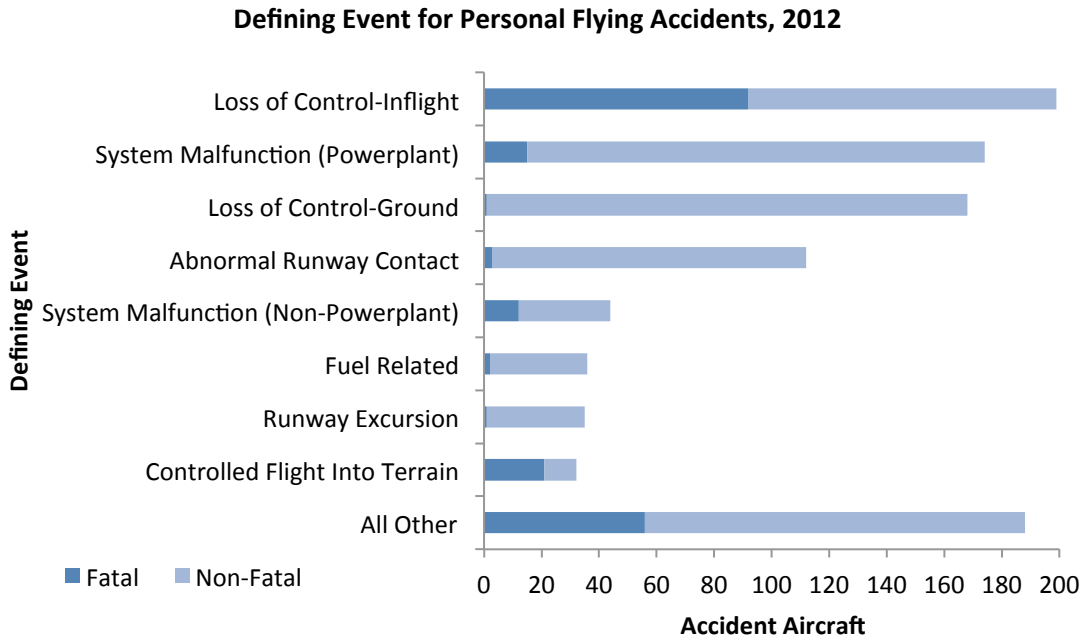

Figure 3: NTSB defining event data for 2012 GA personal flying accidents [2]

There are 26 defining events used by the NTSB (including unknown or undetermined), but just one type – Loss of Control inflight – accounts for nearly half of all fatal personal flying accidents. By their very definition, LoC events are preventable by pilots. Knowing that LoC events are the leading cause of accidents and fatalities in

personal flying, it is important to understand what might cause an inflight loss of control and what is currently being done to prevent these situations.

1.1.3 Loss of Control Events: Causes and Human Factors

Generally speaking, departing from controlled flight involves exceeding the flight envelope of the aircraft. A flight envelope describes the capability of the aircraft in terms of airspeed, altitude, and load factor. Flying outside the envelope may result in aerodynamic stalls, physical damage to the aircraft, aerodynamic spins, and even unrecoverable loss of control. In the discussed LoC events, it is assumed that control either should have been maintained by the pilot or regained after it was lost [3]. This presumption usually excludes events in which control was lost due to some sort of abnormal failure or event (e.g. major wing damage due to weather). Essentially, if the pilot keeps the aircraft within the envelope, control should be maintained.

Several reasons could result in a pilot directing an aircraft out of (or failing to keep it within) its accepted flight envelope. For example, if an instrument in the cockpit (e.g. airspeed indicator) fails, a pilot may be reasonably expected to recognize, troubleshoot, and correct or find alternative solutions for the issue. If the pilot is unable to correct the issue and loses control of the aircraft, this can be considered an LoC event where the pilot should have maintained control. Another common flight environment where LoC is likely to occur is on approach for landing, where a pilot's workload for the tasks at hand can be very high. If the pilot is distracted and lets airspeed drop, or enters a highly banked turn with low airspeed, the low-altitude event can quickly turn into a fatal loss of control. In both of these examples, a pilot would have reasonably been expected to maintain control of his aircraft, as required training exists for instrument failures and

challenging landings. In an LoC situation, appropriate flight control inputs can determine whether a pilot maintains or loses control of the aircraft. There are plenty of scenarios that could lead to a preventable loss of control, but many have one thing in common: a lack of situational awareness.

Situational Awareness (SA) is what allows a pilot to respond appropriately to the conditions in flight. A pilot must be able to recognize key events, understand the meaning of the events, and predict future consequences of control inputs. As Daryl Smith says, "The pilot who sees the change, understands the change, and is able to project what this means for [the] aircraft has high situational awareness" [4]. With high SA, a pilot can determine the correct actions to take before an LoC event turns into an accident.

Maintaining a high level of SA is imperative for a pilot to operate an aircraft safely. Greater training can result in higher levels of SA and result in fewer accidents [5], but occasionally high workloads can overwhelm even seasoned pilots. If a task's requirements exceed the pilot's capabilities, it may be completely neglected or not done properly [6]. Perhaps even worse, a pilot with great abilities may become overconfident and complacent while operating an aircraft. Complacency, referred to as "probably the deadliest of the flying sins" by Richard Collins [5], can put overconfident pilots in unrecoverable operations. To break the loop and ensure pilots are able to recognize potentially dangerous changes in flight conditions, methods to improve SA and compensate for complacency have been implemented throughout aviation's history.

1.2 Current Methods of Prevention

There are several methods, regulations, and aftermarket systems that can aid in preventing LoC events. One method of LoC prevention is the use of a pilot's operating

handbook (POH) for an aircraft, which is a passive defense for LoC incidents. Ideally, through the POH, a pilot is aware of the flight envelope and limitations of the aircraft and can estimate the aircraft's position in the flight envelope using cockpit instrument data. However, in high workload situations, such as approaching a runway to land, pilots continually scan for traffic, communicate with air traffic control, adjust the aircraft's configuration, and are generally less able to pay close attention to instruments in the cockpit. Relying solely on visual instrumentation that indicates proximity to a potential LoC event only increases the pilot's visual scanning and mental workload. Additionally, recalling data from the POH to apply in flight is difficult and mentally inefficient. As a result, aural and visual stall warnings were developed to alert a pilot who has lost focus on the aircraft's flight regime and is nearing aerodynamic stall (i.e. sudden loss of lift).

To prevent LoC due to aerodynamic stall or spin, Federal Aviation Regulations (FARs) require all certified small aircraft to have a 5-knot margin stall warning in wings-level flight [7]. For other specified stalls, a warning is required to give the pilot enough time to react and regain control of the aircraft. However, continued LoC incidents indicate these minimum requirements may offer insufficient warnings for pilots to correct rapidly changing situations that have small safety margins, such as turning the aircraft on final approach to a runway. Additionally, experimental or amateur-built aircraft do not have stall warning standards and may not possess any stall warning method, increasing the potential for an LoC event.

Similar to traditional stall warnings, angle of attack indicators warn a pilot when their aircraft is reaching an excessive angle of attack. These indicators are often graphical

and aural in nature. An example indicator from Advanced Flight Systems, Inc. [8] is shown in Figure 4 below.

Figure 4: Angle of attack indicator from Advanced Flight Systems, Inc. [8] (Used with permission)

The green, yellow, and red lights on the indicator tell a pilot whether or not his aircraft's angle of attack is dangerously high. These indicators are being pushed by the general aviation community for implementation into existing aircraft. The Federal Aviation Administration (FAA) has also recently endorsed their installation as an LoC prevention measure [9]. Unfortunately, if a pilot possesses low situational awareness, these devices do not offer much more protection than traditional stall warnings, as a pilot must look down to see the visual reference. Since these devices are new and widespread adoption has not occurred, their effectiveness in preventing LoC events is not well known.

Highly active, physically installed instrument methods can also be used to prevent loss of control. Fly-by-wire (FBW) systems and their computers can consider the aircraft's current flight condition, pilot control inputs, and the normal flight envelope

before deciding how to position control surfaces. Such systems can limit or ignore dangerous pilot control inputs. “Stick-pusher” systems have also been created for mechanically controlled aircraft [10]. These devices consider the flight envelope of the aircraft and use a servo motor to resist dangerous pilot input in critical flight conditions. While FBW and stick-pusher systems have taken on widespread applications in commercial and military aircraft, they are still in development for general aviation. The prohibitive cost of FBW systems and relative difficulty of retrofitting will likely deter the vast majority of general aviation pilots from installing them in their cockpits.

While current methods to prevent LoC do exist, the consistent accident rate in GA personal flying and the high percentage of LoC events indicate that warnings could be better. For these reasons, it is crucial that more cost-effective methods are developed to complement stall warning devices and enhance pilot situational awareness. To be valuable, a system must provide more time than traditional warnings to safely react to and minimize LoC events. A system that proactively warns pilots of aircraft limitations based on the time they have left to react is needed to enhance SA in the cockpit and reduce LoC events.

1.3 Research Motivation and Objective

The leading cause of accidents and fatalities in general aviation is loss of control in flight. By its very definition, LoC is a preventable situation that a pilot can take actions to avoid. Unfortunately, it seems that pilots too often do not have the situational awareness or perhaps the capability to mitigate situations that are likely to lead to a deadly loss of control. With current methods of mitigation, a significant decline in LoC events has not been observed in available data.

This research addresses the primary cause of fatal general aviation accidents and seeks cost-effective means to enhance the pilot's situational awareness in the early stages of potential LoC events. The primary goal of this research is to develop a proof-of-concept for an active method of warning a pilot of aircraft limitations in flight to supplement traditional stall warning systems. This proof-of-concept will be demonstrated with a software plugin to X-Plane 10, a commercially available flight simulator used by Cessna, Cirrus, NASA, Boeing, and others [11]. In support of the primary goal, this research also aims to understand the simulator's model of a general aviation aircraft and compare its calculations to empirical methods. If the simulator mimics the flight dynamics of a general aviation aircraft well enough, a warning system developed and based upon the simulator's calculations can demonstrate a proof-of-concept for new warning methods. The resulting proof-of-concept would then yield results that should be applicable to actual flight in GA aircraft.

The method demonstrated in this work can use visual and aural warnings and potentially adjust its warning margin based on the potential for fatal loss of control. Such a system can be integrated into current general aviation aircraft using onboard electronic flight information systems (EFIS). For existing aircraft without EFIS, the method can be implemented on a standalone system that would lower training and cost barriers to bring enhanced situational awareness to a wider audience of pilots, including the growing number of experimental or amateur-built aircraft pilots.

Chapter 2: Flight Simulator Comparison with Empirical Data

2.1 X-Plane 10 Introduction

X-Plane 10 is a flight simulator developed by Laminar Research. Much like any flight simulator, X-Plane has a "flight model," which is a mathematical simulation used to calculate an aircraft's flight characteristics. Due to its closed-source nature, little is revealed to the general public about X-Plane's flight model. It is known that X-Plane 10 does not base its flight model on stability derivative tables. Instead, it uses blade element theory [12] to break down aircraft surfaces into small element upon which forces are calculated. There is an emphasis on lifting surfaces, such as the wing and horizontal tail, while the fuselage and other exposed parts of the aircraft are modeled more crudely. Lifting surfaces and the aircraft description are built up in Plane-Maker, an application that comes with X-Plane. Figure 5 on the next page shows a Cessna 172 in X-Plane 10 with lifting vector lines on primary lifting surfaces, including the propeller.

As a common general aviation plane that has been produced since the 1950s, the Cessna 172 is a great example of what the average pilot might fly for personal use. The Cessna 172SP (model 172S) aircraft was used as the basis for analysis in this research. X-Plane 10 is distributed with a model of the Cessna 172SP. Throughout this research, the original and modified versions of the Cessna 172 in X-Plane 10.32 were used.

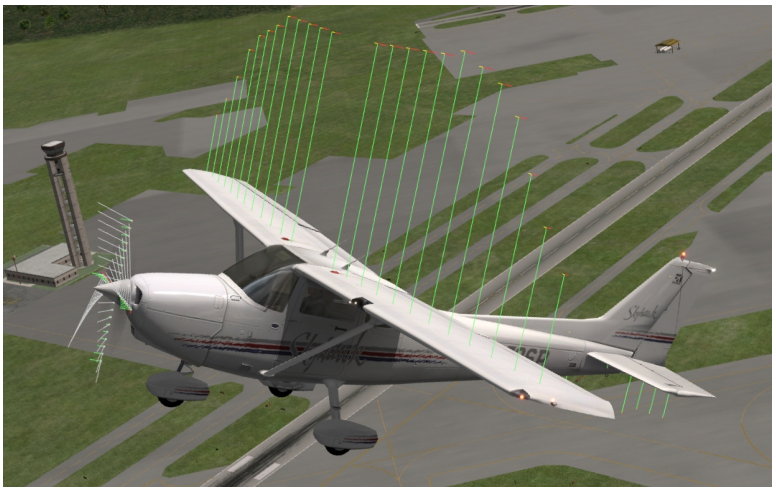

Figure 5: Cessna 172SP flying in X-Plane 10 with flight model visualization

Since the accuracy of the flight model and the Cessna 172 included in X-Plane is not guaranteed, it is critical to understand and compare the results of the model's calculations to what is expected from empirical data. Without a physically reasonable flight model, any warning system developed and tested on the digital flight simulator has little merit in pilot training and real-world use. In the following sections, stability and performance characteristics of X-Plane 10's stock Cessna 172SP are compared primarily to United States Air Force Stability and Control DATCOM (Data Compendium) methods summarized by Roskam [13] and Raymer [14]. DATCOM calculations give stability derivatives that describe how the aircraft responds to changes in airflow and control surface deflections. Existing data for the Cessna 172's stability derivatives was not used due to geometry differences between X-Plane's model and the real aircraft.

2.2 Aircraft Geometry and Empirical Calculations

2.2.1 X-Plane Cessna 172SP Model Reference

The geometric and performance data that constructs the Cessna 172SP is available in a digital file that is viewable in the X-Plane companion program called Plane-Maker. Plane-Maker takes geometric, airfoil, performance, systems, and other aircraft parameters to create an aircraft (.acf) file. X-Plane uses the data that is given in this file to construct the aircraft and place it in the flight model each time an aircraft is loaded into X-Plane. Unless otherwise noted, the stock (unmodified) version of the Cessna 172SP that is included with X-Plane 10.32r1 was used as a reference model for comparison purposes. Equivalent wing, horizontal tail, and vertical tail geometry were obtained using the graphical methods from Roskam [13] with geometric data from Plane-Maker as reference. The creation and usage of equivalent geometry is necessary for empirical-based formulas (such as DATCOM) that do not handle complicated geometry well.

2.2.2 Equivalent Wing Geometry

X-Plane 10 divides lifting surfaces up into separate panels and then calculates the forces on each panel separately using blade element theory. This finite breakup allows X-Plane's flight model to handle many less calculations for otherwise very complicated geometry. For more explanation, see the Figures in Appendix B.

While this finite element process is convenient for achieving good flight characteristics in the X-Plane model, it is not convenient for performing empirical calculations to estimate stability derivatives based on geometry. Using the details from Plane-Maker and to-scale graphics, equivalent geometry was derived using graphical

estimation methods from Roskam's Chapter 2 [13]. The wing was estimated as a trapezoidal shape that preserved X-Plane 10's values of surface area, aspect ratio, tip chord, total span, and approximate leading edge geometry. The results from the process are summarized in Table 2 and Figure 6 below.

Table 2: Equivalent wing geometry summary

$b = 39.36$ ft	$\Lambda_{LE} = 3.28^\circ$
$S = 188.6$ ft^2	$\Lambda_{c/4} = 1.5^\circ$
$\lambda = 0.602$	$\Lambda_{c/2} = -0.23^\circ$
$c_r = 5.98$ ft	$\bar{c}_w = 4.95$ ft
$c_t = 3.60$ ft	$A = 8.214$

The mean aerodynamic chord of the wing was calculated using Equation 1 [14]:

$$\bar{c}_w = \frac{2}{3} c_r \left[\frac{1+\lambda+\lambda^2}{1+\lambda}\right] \quad (1)$$

Where λ is the taper ratio, which is defined by the ratio of the root and tip chord lengths:

$$\lambda = \frac{c_r}{c_t} \quad (2)$$

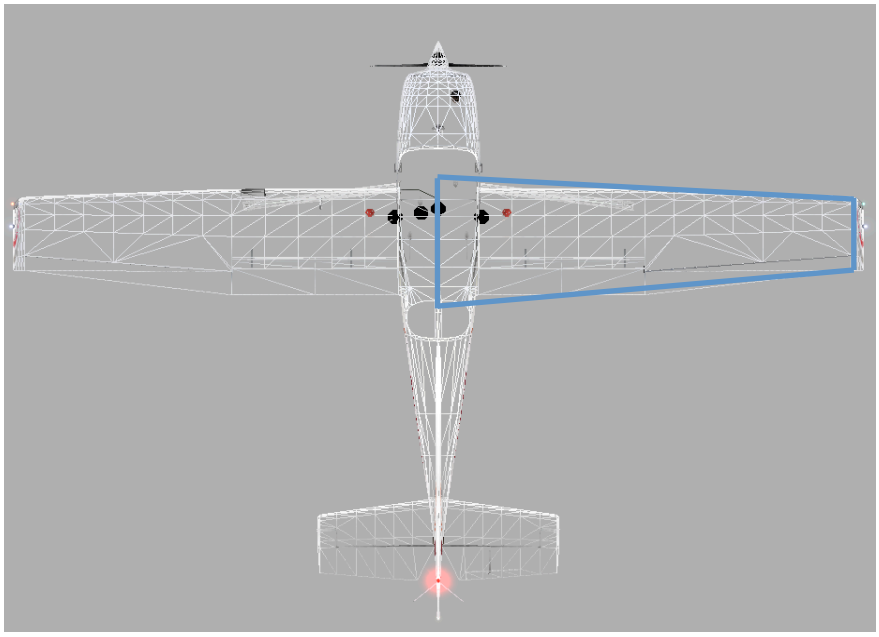

Figure 6: Equivalent wing geometry (not to scale)

It should be noted that the surface area and span of the Cessna 172's wing in X-Plane 10 is larger than the actual aircraft [15]. While the exact reason for the discrepancy is unknown, the X-Plane focus on lifting surfaces and lack of precise fuselage modeling may be involved. Where discrepancies exist between the X-Plane Cessna 172SP and the actual aircraft, X-Plane's values will be used to directly compare the flight model to the graphical and empirical calculations.

2.2.3 Equivalent Empennage Geometry

Similar to the wing geometry in Section 2.2.2 above, equivalent horizontal and vertical tail geometry was derived using X-Plane information and Roskam's equivalent geometry methods [13]. Where needed, to-scale prints were used to derive dimensions that were not readily available in Plane-Maker. The horizontal tail was estimated as a trapezoidal shape that preserved X-Plane 10's values of surface area, aspect ratio, tip chord, total span, and approximate leading edge geometry. The elevator chord ratio (c_e/c_{HT}) was 0.40. A summary of the process is provided in Table 3 below and Figure 7 on the following page.

Table 3: Equivalent horizontal tail geometry summary

$b_{HT} = 11.16$ ft	$\Lambda_{LE} = 7.15^{\circ}$
$S_{HT} = 20.35$ ft^2	$\Lambda_{c/4} = 5.00^{\circ}$
$\lambda_{HT} = 0.623$	$\Lambda_{c/2} = 2.84^{\circ}$
$c_r = 4.49$ ft	$\bar{c}_{HT} = 3.713$ ft
$c_t = 2.8$ ft	$A_{HT} = 6.12$

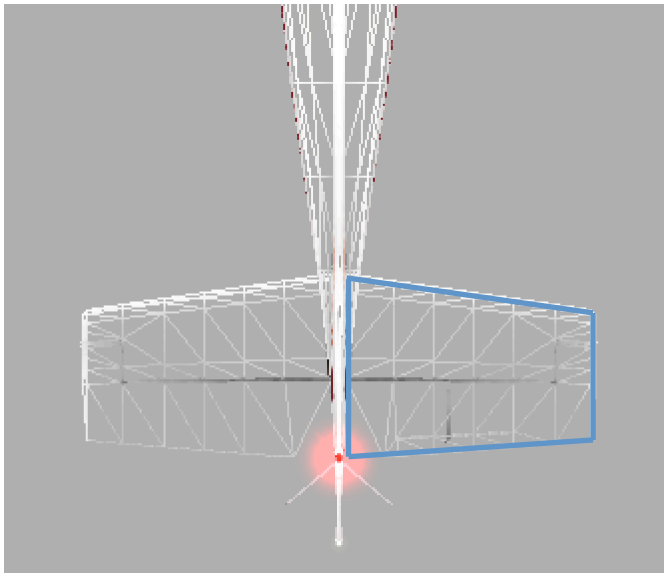

Figure 7: Equivalent horizontal tail geometry visualization (not to scale)

The horizontal tail span in X-Plane is actually slightly smaller than the span on the real aircraft [15]. However, it does not appear that the gap in the horizontal tail for elevator travel is modeled with any accuracy in X-Plane.

Equivalent vertical tail geometry was also created using graphical methods similar to the wing and horizontal tail. Due to the Cessna 172's large dorsal fin, the vertical tail was modeled in two separate pieces in X-Plane (see Figure B-3 in Appendix B). These two pieces were combined into one equivalent vertical tail. A summary of the geometry results is provided in Table 4 below and Figure 8 on the next page.

Table 4: Equivalent vertical tail geometry summary

$b_{VT} = 5.59$ ft	$\lambda_{VT} = 0.4048$
$S_{VT} = 22.79$ ft^2	$\Lambda_{c/4} = 37.0^\circ$
$c_r = 5.81$ ft	$\bar{c}_{VT} = 4.321$ ft
$c_t = 2.35$ ft	$A_{VT} = 1.37$

Figure 8: Equivalent vertical tail geometry visualization (not to scale)

2.2.4 Center of Gravity Location

Other geometric values were taken from the Cessna 172 model in Plane-Maker, including the nominal center of gravity location. The center of gravity location, taken from the Cessna 172 model in Plane-Maker, is 3 inches aft of the wing quarter-chord at the root, which was taken to be 1.0 ft aft of the equivalent wing leading edge. This center of gravity location, x_{cg}, was used for all stability derivative calculations and X-Plane flight test extractions.

2.2.5 Longitudinal Stability Derivatives

Basic longitudinal stability derivatives were calculated using equivalent geometry and methods from Roskam [13] and Raymer [14]. These parameters are summarized in Table 5, with detailed explanations on how they were obtained discussed below.

Table 5: Summary of empirical-based longitudinal stability derivatives

C_{L_α}	C_{m_α}	$C_{L_{\delta F}}$	$C_{M_{\delta F}}$	$C_{L_{\delta E}}$	$C_{M_{\delta E}}$
0.0884	-0.0256	0.0151	-0.00394	0.00613	-0.0188

Note: all terms are in deg^{-1}

Lift-Curve Slope

The lift-curve slope (C_{L_α}) was estimated using Equation 3 [13]:

$$C_{L_\alpha} = C_{L_{\alpha_{WB}}} + C_{L_{\alpha_H}} \eta_{HT} \frac{S_H}{S} \left(1 - \frac{d\varepsilon}{d\alpha}\right) \tag{3}$$

Using the methods described in Roskam [13], $C_{L_{\alpha_{WB}}}$ and $C_{L_{\alpha_H}}$ were also estimated:

$$C_{L_\alpha} = \frac{2\pi A}{2 + \sqrt{\frac{A^2\beta^2}{\kappa^2} + \frac{tan^2 \Lambda_{c/2}}{\beta^2} + 4}} \tag{4}$$

where β is a compressibility correction [13]:

$$\beta = \sqrt{1 - M^2} \tag{5}$$

and κ is the ratio of the 2D airfoil lift curve slope to theory [14]:

$$\kappa = \frac{C_{\ell_\alpha}}{2\pi} \; or \; \frac{C_{\ell_\alpha}}{360^\circ} \tag{6}$$

Many small general aviation aircraft fly slowly enough that compressibility effects can be ignored (i.e. $\beta = 1$), however a small amount of compressibility effects were considered. With a Cessna 172's cruise speed a little over 100 mph at Sea Level, $M = 0.15$ was used where applicable.

Using Equations 3-6, equivalent wing geometry from Section 2.2.2, and the parameters given in Table 6 below, C_{L_α} for the Cessna 172SP was calculated to be 0.0884 deg^{-1}.

Table 6: Parameters used for lift-curve slope calculations

Parameter	Value	Description
S_{HT}	20.35 ft^2	Horizontal tail area
η_{HT}	0.9	Horizontal tail dynamic pressure ratio (q_{HT}/q_∞) assumed with guidance of Roskam [13] and Raymer [14]
$C_{\ell_{\alpha_w}}$	0.101 deg^{-1}	NACA 2412 airfoil lift curve slope [16]
$C_{\ell_{a_{HT}}}$	0.100 deg^{-1}	NACA 0006 airfoil lift curve slope [16]
$\frac{\partial \varepsilon}{\partial \alpha}$	0.33	Change in downwash angle with change in angle of attack (calculated with Roskam's methods [13])
M	0.15	Nominal Mach Number for Cessna 172S flight

Pitching Moment Curve Slope

The pitching moment curve slope (C_{M_α}) was estimated using Equation 7 [13]:

$$C_{M_\alpha} = \frac{dC_M}{dC_L} C_{L_\alpha} \tag{7}$$

The term $\frac{\mathrm{dC_M}}{\mathrm{dC_L}}$ is known as the static margin of an aircraft and is given by:

$$\frac{dC_M}{dC_L} = \bar{x}_{cg} - \bar{x}_{np} \tag{8}$$

Where ($\bar{x}_{cg} - \bar{x}_{np}$) is the mean aerodynamic chord (MAC) normalized distance between the longitudinal center of gravity and longitudinal location of the neutral point (i.e. the aerodynamic center of the aircraft). Normalizing distances with the wing MAC, $\bar{c}$, is common notation for the longitudinal axis stability derivatives as shown:

$$\bar{x}_{cg} = \frac{x_{cg}}{\bar{c}_w} \tag{9}$$

In this work, both x_{np} and x_{cg} are measured from the leading edge of the equivalent wing's root. If the neutral point location is forward of $\bar{x}_{cg}$, then the aircraft is unstable. The neutral point is calculated by using Roskam's [13] and Raymer's [14] methods while ignoring thrust effects:

$$\bar{x}_{np} = \frac{C_{L_{\alpha_{WB}}}\bar{x}_{ac_{WB}} - C_{M_{\alpha_{fus}}} + C_{L_{\alpha_{HT}}}\eta_{HT}\frac{S_{HT}}{S}\bar{x}_{ac_{HT}}\left(1-\frac{\partial\varepsilon}{\partial\alpha}\right)}{C_{L_{\alpha_{WB}}} + C_{L_{\alpha_{HT}}}\eta_{HT}\frac{S_{HT}}{S}\left(1-\frac{\partial\varepsilon}{\partial\alpha}\right)} \tag{10}$$

A summary of the parameters used in calculating the neutral point location is provided in Table 7 below:

Table 7: Parameters used for calculating neutral point

Parameter	Value	Description
$C_{M_{\alpha_{fus}}}$	0.00437 deg^{-1}	Fuselage increment to change in coefficient of moment with change in angle of attack [14]
η_{HT}	0.9	Horizontal tail dynamic pressure ratio (q_{HT}/q_{∞})
e	0.8	Oswald efficiency factor
$\bar{x}_{ac_{WB}}$	0.357	x-location (rearward positive) of wing, referenced to leading edge of equivalent wing root
$\bar{x}_{ac_{HT}}$	3.39	x-location (rearward positive) of horizontal tail's aerodynamic center, referenced to leading edge of equivalent wing root
$\frac{\partial\varepsilon}{\partial\alpha}$	0.33	Change in downwash angle with change in angle of attack (calculated with Roskam's methods [13])

The aerodynamic center (AC) of the wing and horizontal tails was placed on the quarter-chord line. The Y-distance to the AC was calculated using Equation 11 below [14] and the distance to the leading edge of the equivalent geometry wing was measured to get $x_{ac_{WB}}$ and $x_{ac_{HT}}$.

$$\bar{Y} = \frac{b}{6}\frac{1+2\lambda}{1+\lambda} \tag{11}$$

Using the processes described above, Equations 7-11, and the equivalent wing and horizontal tail geometry, C_{M_α} = -.0244 deg^{-1}. Daniel Raymer [14] suggests that static margin will increase with high-wing aircraft designs. With the Cessna 172SP design, the static margin (and thus the magnitude of C_{M_α}) may be expected to increase around 6%, bringing C_{M_α} to -0.0256

Flap Term Calculations

Lift and moment increments due to flap deflection, $C_{L_{\delta F}}$ and $C_{M_{\delta F}}$, were calculated using Equations 12 and 13 and methods from Roskam [13] and Raymer [14]:

$$C_{L_{\delta F}} = C_{\ell_{\delta F}} \left(\frac{C_{L_\alpha}|_M}{C_{\ell_\alpha}|_M} \right) \left[\frac{(\alpha_\delta)_{C_L}}{(\alpha_\delta)_{C_\ell}} \right] K_b \tag{12}$$

$$C_{M_{\delta F}} = -C_{L_{\delta F}} (\bar{x}_{cp} - \bar{x}_{cg}) \tag{13}$$

A summary of the parameters used in calculating $C_{L_{\delta F}}$ and $C_{M_{\delta F}}$ is given in Table 8 below. For direct comparison of the calculated flap coefficient terms available in X-Plane, calculations were based on an assumed flap deflection (δF) of 40˚.

Table 8: Parameters used for calculating flap coefficients

Parameter	Value	Description
$C_{\ell_{\delta F}}$	0.0364 (deg^{-1})	Theoretical flap-lift effectiveness [13]
$\frac{C_{L_\alpha}\|_M}{C_{\ell_\alpha}\|_M}$	0.800 (deg^{-1})	Ratio of lift curve slope of the unflapped surface to airfoil section lift curve slope, corrected for Mach effects [13]
$\frac{(\alpha_\delta)_{C_L}}{(\alpha_\delta)_{C_\ell}}$	1.04	Ratio of 3D flap effectiveness parameter to 2D flap effectiveness parameter, function of surface aspect ratio and theoretical value of $(\alpha_\delta)_{C_\ell}$ [13]
K_b	0.5	Flap span factor, evaluated at 40˚ [13]
$\bar{x}_{cp}$	0.462	Center of pressure of the flap lift increment [14]

It should be noted that Roskam's DATCOM methods assume a sealed gap plain flap [13]. Raymer suggests as much as a 15% reduction in terms for non-sealed surfaces [14]. This reduction was not applied for the flaps because the Cessna 172 has slotted flaps that exhibit a slight Fowler flap motion. The final results of empirical calculations for $C_{L_{\delta F}}$ and $C_{M_{\delta F}}$ were 0.0151 deg^{-1} and -0.00394 deg^{-1}, respectively.

Elevator Term Calculations

Elevator coefficients are calculated in a similar manner to the flap terms above using Equations 14 and 15 from Roskam [13]. This is possible because the elevator essentially acts as a plain flap on the horizontal tail.

$$C_{L_{\delta E}} = C_{\ell_{\delta E}} \left(\frac{C_{L_\alpha}\big|_M}{C_{\ell_\alpha}\big|_M} \right) \left[\frac{(\alpha_\delta)_{C_L}}{(\alpha_\delta)_{L_\ell}} \right] K_b \tag{14}$$

$$C_{M_{\delta E}} = -C_{L_{\delta E}} \frac{l_{HT}}{\bar{c}} \tag{15}$$

A summary of the parameters used in calculating $C_{L_{\delta E}}$ and $C_{M_{\delta E}}$ is given in Table 9 below.

Table 9: Parameters used for calculating elevator coefficients

Parameter	Value	Description
$C_{\ell_{\delta E}}$	0.0744 (deg^{-1})	Theoretical elevator-lift effectiveness [13]
$\frac{C_{L_\alpha}\big\|_M}{C_{\ell_\alpha}\big\|_M}$	0.7443	Ratio of lift curve slope of unflapped ($\delta E = 0°$) surface to airfoil section lift curve slope, corrected for Mach effects [13]
$\frac{(\alpha_\delta)_{C_L}}{(\alpha_\delta)_{C_\ell}}$	1.025	Ratio of 3D elevator effectiveness parameter to 2D elevator effectiveness parameter, function of surface aspect ratio and theoretical value of $(\alpha_\delta)_{C_\ell}$ [13]
K_b	1.0	Elevator span factor [13]
l_{HT}	15.2 ft	Tail arm (distance between aerodynamic centers of wing and horizontal tail)

Since elevator deflections are often used to make smaller adjustments, an assumed elevator deflection (δE) of only 10˚ was used. The final results of empirical calculations for $C_{L_{\delta E}}$ and $C_{M_{\delta E}}$ were 0.00613 deg^{-1} and -0.0188 deg^{-1}, respectively.

2.2.6 Lateral-Directional Stability Derivatives

Two lateral-directional stability derivatives were chosen for empirical calculation and X-Plane comparison. Lateral-directional static stability is indicated by the aircraft's response to sideslip (β). The yawing moment due to sideslip (C_{N_β}) and the rolling moment due to sideslip (C_{ℓ_β}) were estimated using Equations 16 and 17 below from Raymer [14] and equivalent geometry of the vertical tail and wings.

$$C_{N_\beta} = C_{N_{\beta_w}} + C_{N_{\beta_{fus}}} + C_{N_{\beta_{VT}}} \tag{16}$$

$$C_{\ell_\beta} = C_{\ell_{\beta_w}} + C_{\ell_{\beta_{VT}}} \tag{17}$$

The vertical tail provides the largest contribution to lateral-directional stability. The vertical tail terms $C_{N_{\beta_{VT}}}$ and $C_{\ell_{\beta_{VT}}}$ are given by Equations 18 and 19 below from Raymer [14].

$$C_{N_{\beta_{VT}}} = C_{F_{\beta_{VT}}} \frac{\partial \beta_{VT}}{\partial \beta} \eta_{VT} \frac{S_{VT}}{S_w} \left(\bar{x}_{ac_{VT}} - \bar{x}_{cg}\right) \tag{18}$$

$$C_{\ell_{\beta_{VT}}} = C_{F_{\beta_{VT}}} \frac{\partial \beta_{VT}}{\partial \beta} \eta_v \frac{S_{VT}}{S_w} \bar{Z}_{VT} \tag{19}$$

In lateral-directional equations, normalized ("bar") terms are found by dividing the dimensional distance by the wingspan:

$$\bar{x}_{ac_{VT}} = \frac{x_{ac_{VT}}}{b_w} \tag{20}$$

Parameters used in the calculation of C_{N_β} and C_{ℓ_β} are given in Table 10 below. Some lateral-directional terms, such as the $C_{N_{\beta_w}}$ in Equation 16, are dependent on flight condition. Where applicable, these parameters were evaluated at the flight conditions most similar to those experienced when extracting sideslip derivatives from X-Plane (see Section 2.3.2).

Table 10: Parameters used for calculating sideslip derivatives

Parameter	Value	Description
$C_{F_{\beta_{VT}}}$	0.0314 (deg^{-1})	Vertical tail lift curve slope
$\frac{\partial \beta_v}{\partial \beta}\eta_{VT}$	1.245	Vertical tail sideslip derivative times the local dynamic pressure ratio [14]
$\bar{x}_{ac_{VT}}$	0.4326	Location of vertical tail aerodynamic center, normalized with the wing span, referenced to leading edge of equivalent wing
$\bar{Z}_{VT}$	0.0617	Vertical distance from c.g. position to vertical tail aerodynamic center [14]

The final results of empirical calculations for C_{N_β} and C_{ℓ_β} are given in Table 11 below.

Table 11: Empirical estimations of lateral-directional sideslip derivatives

C_{N_β} (deg^{-1})	0.00120
C_{ℓ_β} (deg^{-1})	-0.00029

The calculated C_{N_β} is very near (but slightly lower) than the value that is given in Raymer's text for a Cessna 182, 0.00131 deg^{-1}. The Cessna 182 is of very similar design but slightly larger than the 172. The flight condition in which the Cessna 182 C_{N_β} was calculated is not known. A different flight condition and slightly different geometry may account for the minor discrepancy in values.

2.3 Extracted Data from X-Plane 10 Flight Tests

Data was exported from X-Plane using "Data-Out" in the X-Plane 10 software. A screenshot of X-Plane's Data-Out options is given in Figure 9 below. The Data-Out functionality allows a user to export many variables from the Flight Model. For the purposes of this research, X-Plane was requested to write variables to a text file at a rate of 50 Hz. With X-Plane graphics frames running between 20 and 40 Hz and the flight model computing 2-3 times per graphics frame, this requests that X-Plane exports nearly every frame. In practice, it is likely that some computed flight model frames could be lost. Extremely high resolution of the flight model is not required for this research, so the built-in Data-Out functionality was considered adequate.

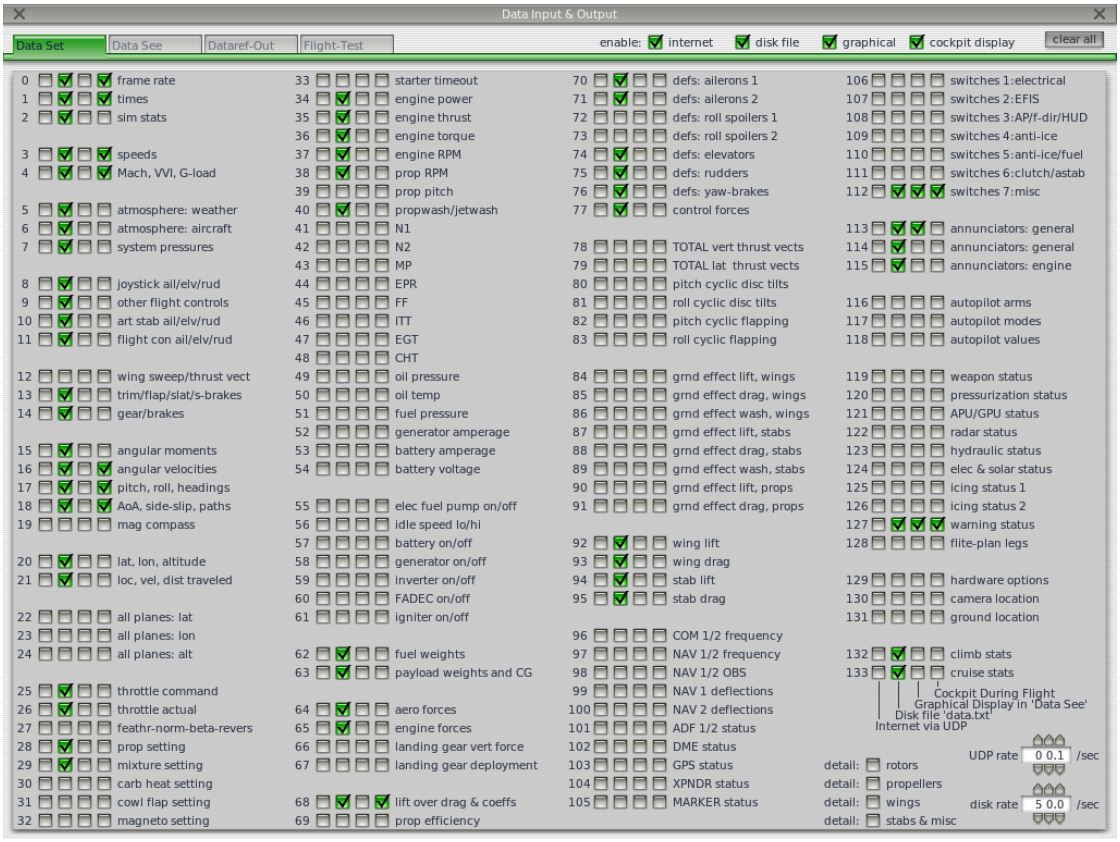

Figure 9: X-Plane data-out options

2.3.1 Longitudinal Flight Test Extractions

As one of the most basic aerodynamic parameters, the lift curve slope (C_{L_α}) for the Cessna 172SP was evaluated in X-Plane. The pitching moment curve slope (C_{m_α}), offers an understanding of the static stability of an aircraft. If a simulator models an excessively stable or less stable aircraft, the simulated handling qualities may be significantly different than a pilot would expect in real life. Elevator terms $C_{L_{\delta E}}$ and $C_{m_{\delta E}}$ show how the total lift and moment of the aircraft change with elevator deflection. When compared to DATCOM results, these terms indicate the elevator's effectiveness in the simulator. These longitudinal coefficients have been extracted from X-Plane because of their relevance to the development of a Loss of Control warning system and because they offer basic physical comparison of simulated flight model results with empirical data. Additionally, flap coefficients were extracted from Plane-Maker.

Lift Curve Slope

The change in lift coefficient with respect to angle of attack (C_{L_α}) was extracted from X-Plane by a smooth sweep of power settings while holding altitude. The aircraft was held at 4,000 ft in a calm standard atmosphere. It was initially trimmed for Straight, Level, Unaccelerated Flight (SLUF) at approximately 100 KIAS, but no further trim adjustments were made. The aircraft's power setting was slowly increased to maximum and then slowly reduced until just before expected stall. A scatter plot of the corresponding C_L and α pairs is shown in Figure 10 on the following page.

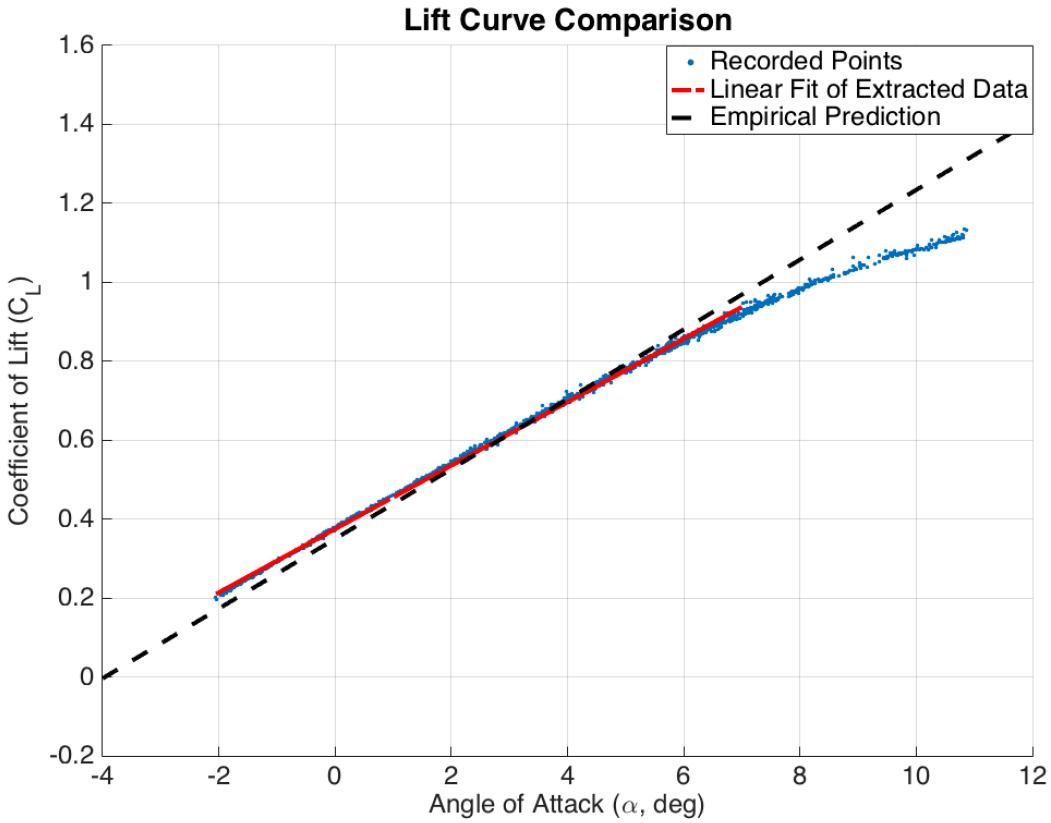

Figure 10: Cessna 172 lift curve extraction from X-Plane 10

Near stall the lift curve slope becomes nonlinear, which is typical of a wing's lift curve. Aerodynamic stall begins to occur around and after $\alpha = 11^{\circ}$. In forming the extracted C_{L_α}, the linear region of the lift curve was considered. This region is found below $\alpha = 8^{\circ}$ as shown in Figure 10. A linear fit of all values below $\alpha = 7^{\circ}$ was selected for the extraction of C_{L_α}. The results are presented in Table 12 below.

Table 12: Extracted lift curve slope parameters

C_{L_α} (deg^{-1})	0.0804
$C_{L_{\alpha=0^{\circ}}}$	0.375

Note: $C_{L_{\alpha=0^{\circ}}}$ is the coefficient of lift that is generated when $\alpha = 0^{\circ}$.

Moment Curve Slope

The change in longitudinal moment coefficient with respect to angle of attack was extracted by observing the aircraft's response to an instantaneous change in pitch. In X-Plane, the flight model calculates the angle of attack on different geometry surfaces. Changing the aircraft's angle of attack is most easily accomplished by instantaneously changing its pitch.

To change the pitch in X-Plane, a custom Cessna 172SP cockpit panel and software plugin were developed. The cockpit panel modification, as shown in Figure 11 below, allowed the pilot to choose different changes in rotation about the pitch, roll, and heading axes ($\Delta\theta,\ \Delta\phi,\ \Delta\psi$), which would be executed by the software plugin when the "Execute Change" button was pressed.

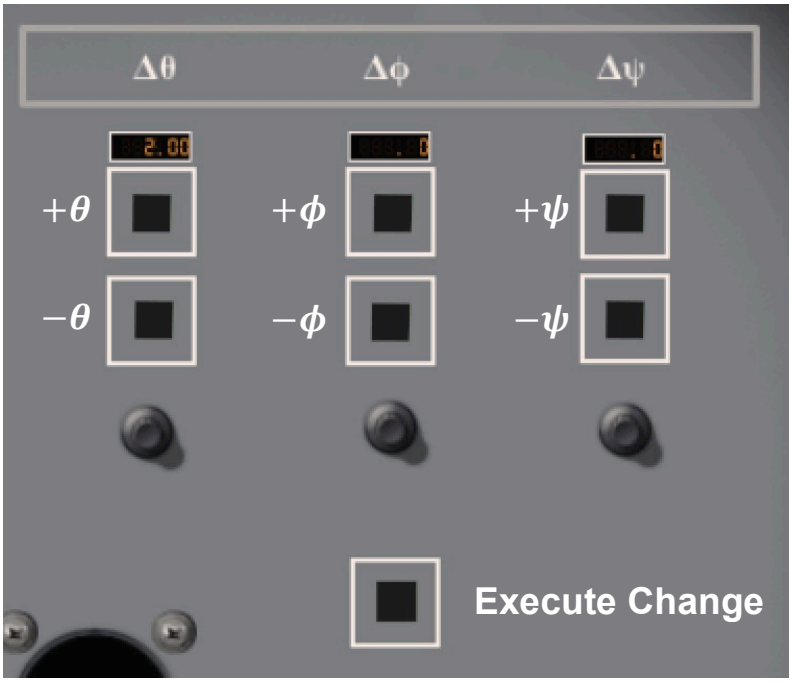

Figure 11: Cockpit panel modifications for change in orientation

In order to change the pitch angle correctly, the plugin had to consider the orientation of the Cessna 172 in X-Plane's flight model. The aircraft's orientation, including pitch, roll, and heading (θ, ϕ, ψ) is recorded as a quarternion instead of Euler Angles or rotation matricies. The quaternion is stored as a four-variable array in the flight model, which is described by Equations 21a-d as given from the X-Plane Software Development Kit (SDK) [17]:

$$q[0] = \cos\psi \cos\theta \cos(\phi) + \sin(\psi)\sin(\theta)\sin(\phi) \tag{21a}$$

$$q[1] = \cos\psi \cos\theta \sin(\phi) - \sin(\psi)\sin(\theta)\cos(\phi) \tag{21b}$$

$$q[2] = \cos\psi \sin\theta \cos(\phi) + \sin(\psi)\cos(\theta)\sin(\phi) \tag{21c}$$

$$q[3] = -\cos\psi \sin\theta \sin(\phi) + \sin(\psi)\cos(\theta)\cos(\phi) \tag{21d}$$

Each time the plugin was commanded to execute an orientation change, it considered the current orientation of the aircraft (θ, ϕ, ψ) and the requested changes $(\Delta\theta, \Delta\phi, \Delta\psi)$. It then calculated a new quaternion using Equations 21a-d and changed the orientation in the flight model.

For the purposes of extracting C_{M_α}, only the $\Delta\theta$ option was used to instantaneously change the aircraft's pitch and thus angle of attack in the flight model. The aircraft was held at 100 KIAS in SLUF at 4,000 ft in a calm standard atmosphere. When SLUF was established, the aircraft was displaced a designated value in pitch. When the aircraft restabilized near the initial altitude, the process was repeated.

Figure 12 on the following page is a time-history example of a C_{M_α}extraction flight test. In this example, a pitch increase of 5˚ was commanded by the plugin, resulting in nearly a 5˚ change in angle of attack.

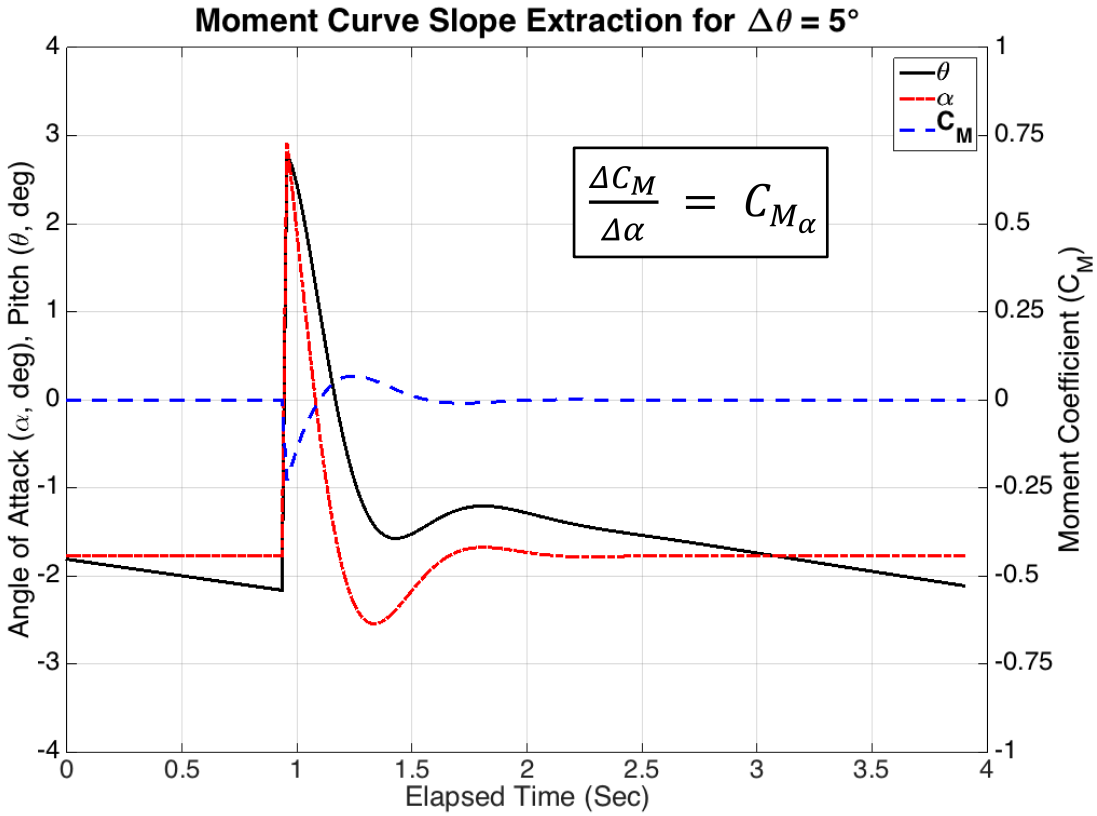

Figure 12: Moment curve slope extraction, X-Plane time history

This process was completed 12 times with positive increases in pitch forced upon the flight model. The stability derivative C_{M_α} was approximated by using the relation:

$$\frac{\Delta C_M}{\Delta \alpha} = C_{M_\alpha} = \frac{M}{qS\bar{c}} \tag{22}$$

The lowest value of C_M and the highest value of α were identified by MATLAB scripts and used in Equation 22 above. A linear trend was observed for the extracted C_{M_α} based on the commanded magnitudes of $\Delta\theta$ and the resulting flight model $\Delta\alpha$. This trend is shown in Figure 13 on the following page.

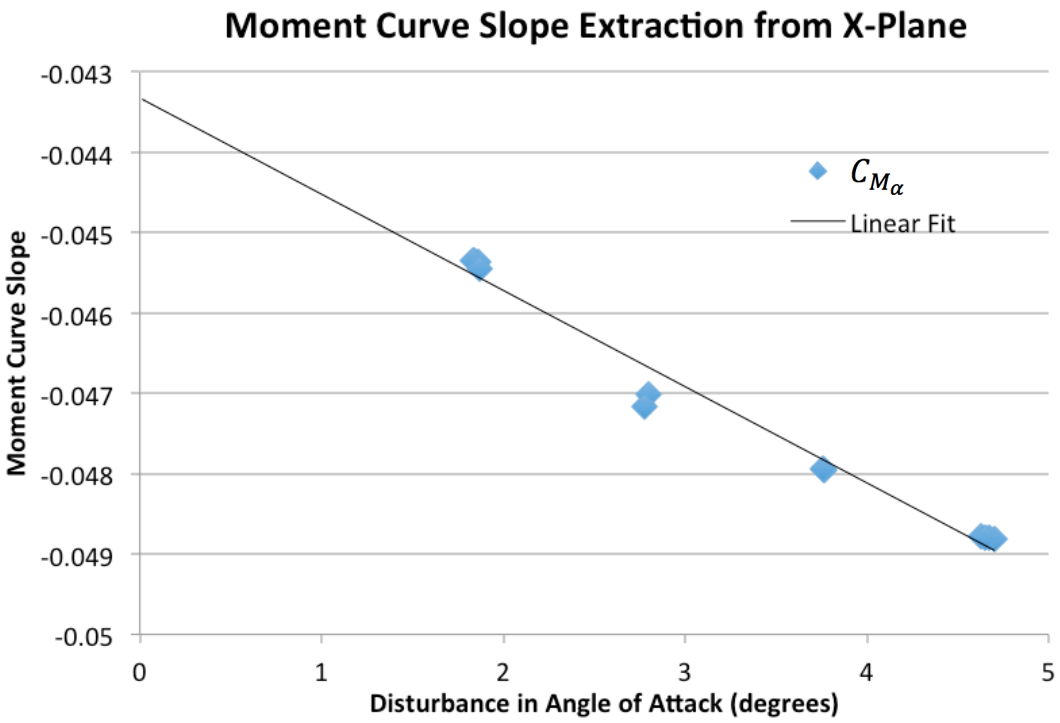

Figure 13: Moment curve slope trend with varying changes in angle of attack

Using a linear fit of extracted C_{M_α} data, the intercept of the ordinate was used as the expected value for C_{M_α}. A linear fit intercept was used instead of a statistical average because stability derivatives are typically considered for a particular equilibrium flight condition. In this case, the equilibrium point for SLUF is a 0˚ disturbance in α. The final calculated C_{M_α} was -0.0433 deg^{-1}.

Elevator Increments to Moment and Lift Coefficients

The change in lift coefficient with respect to elevator deflection ($C_{L_{\delta E}}$) and the change in moment coefficient with respect to elevator deflection ($C_{M_{\delta E}}$) were extracted from X-Plane by observing the aircraft's response to a step input of elevator deflection. The aircraft's step elevator response, as in control theory, is the dynamic response of the

aircraft when the elevator is instantaneously deflected to a certain value (away from the trim point). An example time history of this process is shown in Figure 14 below.

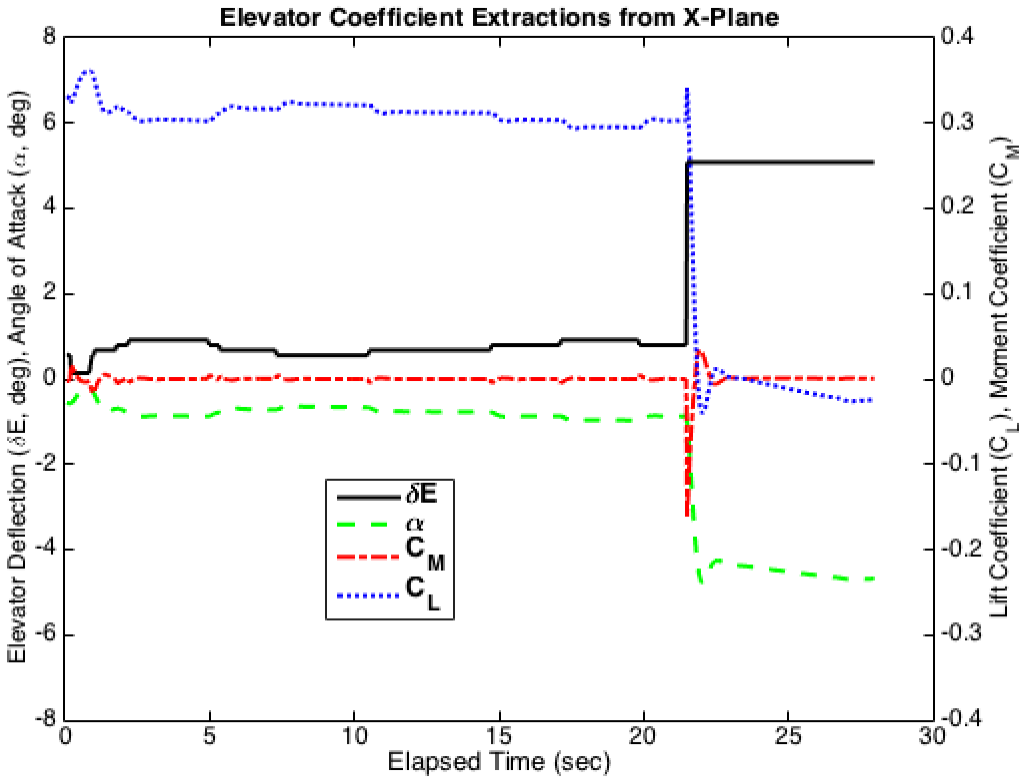

Figure 14: Cessna 172SP time response to positive elevator deflection step change

In the above simulated flight test, the aircraft was manually flown and trimmed for SLUF at approximately 4,000 ft in a calm standard atmosphere. The simulator was paused and the elevator deflection was changed in the flight model. The simulation was then resumed, and the elevator deflection was held constant. For consistency, all stability augmentation was turned off and control response was set to completely linear in X-Plane's settings.

Seven aircraft nose down (positive $\Delta\delta E$) elevator step changes were made. The aircraft was reset to its trim state before each step change in elevator. The data was

analyzed in MATLAB, where the changes $\Delta\delta E$, ΔC_L, and ΔC_M were identified. The details of the flight test results are given in Table 13 below.

Table 13: X-Plane elevator coefficients extraction data

$\Delta\delta E$	0.857˚	1.71˚	2.57˚	4.29˚	6.43˚	8.58˚	10.3˚
$\frac{\Delta C_L}{\Delta\delta E}$	0.00811	0.00790	0.00796	0.00897	0.00896	0.00844	0.00881
$\frac{\Delta C_M}{\Delta\delta E}$	-0.038	-0.037	-0.037	-0.038	-0.038	-0.038	-0.037

Given the consistency of results for $\frac{\Delta C_L}{\Delta\delta E}$ and $\frac{\Delta C_m}{\Delta\delta E}$, the X-Plane results were averaged together for all $\Delta\delta E$. The results are presented in Table 14 below.

Table 14: Extracted elevator coefficient parameters

$C_{L_{\delta E}}$ (deg^{-1})	0.0085
$C_{M_{\delta E}}$ (deg^{-1})	-0.0377

Flap Coefficients

The creators of the Cessna 172SP model manually entered certain flap coefficients in Plane-Maker. The flap coefficients appear to be for the maximum flap deflection allowed in the Cessna 172SP model (40˚). It is assumed, but not fully understood, that X-Plane does a coefficient interpolation for non-maximum flap deflections. The flap coefficients and other relevant flap parameters are given in Table 15 below.

Table 15: X-Plane Cessna 172SP flap parameters for 40˚ deflection

Flap Chord	26%
Flap Semi-Span	7.75 ft
C_{L_F}	0.914
C_{D_F}	0.059
C_{M_F}	-0.282

2.3.2 Lateral-Directional Flight Test Extractions

The angle of sideslip derivatives for yawing moment (C_{N_β}) and rolling moment (C_{ℓ_β}) were extracted from X-Plane by observing the aircraft's response to an instantaneous change in heading. These two derivatives were chosen for X-Plane extraction because they indicate yaw and roll stability, respectively. The impulse change in heading was performed using the custom development cockpit and software plugin for flight model changes as described in Section 2.3.1 above. As before, Equations 21a-d were utilized to execute the change in the flight model.

For the purposes of extracting both C_{N_β} and C_{ℓ_β}, only the $\Delta\psi$ (change in heading) functionality was used in the custom cockpit (see Figure 11). The aircraft was trimmed and held at 100 KIAS in SLUF at 4,000 ft in a calm standard atmosphere. As with the longitudinal extractions, the aircraft was displaced a designated value in heading when SLUF was established. After the impulse displacement, a time history was recorded for a few seconds, SLUF re-established, and another displacement was performed.

Figure 15 on the following page is a time-history example of a C_{N_β} and C_{ℓ_β} extraction flight test. In this example, a heading increase of 4˚ was commanded by the plugin, resulting in nearly a 4˚ change in sideslip.

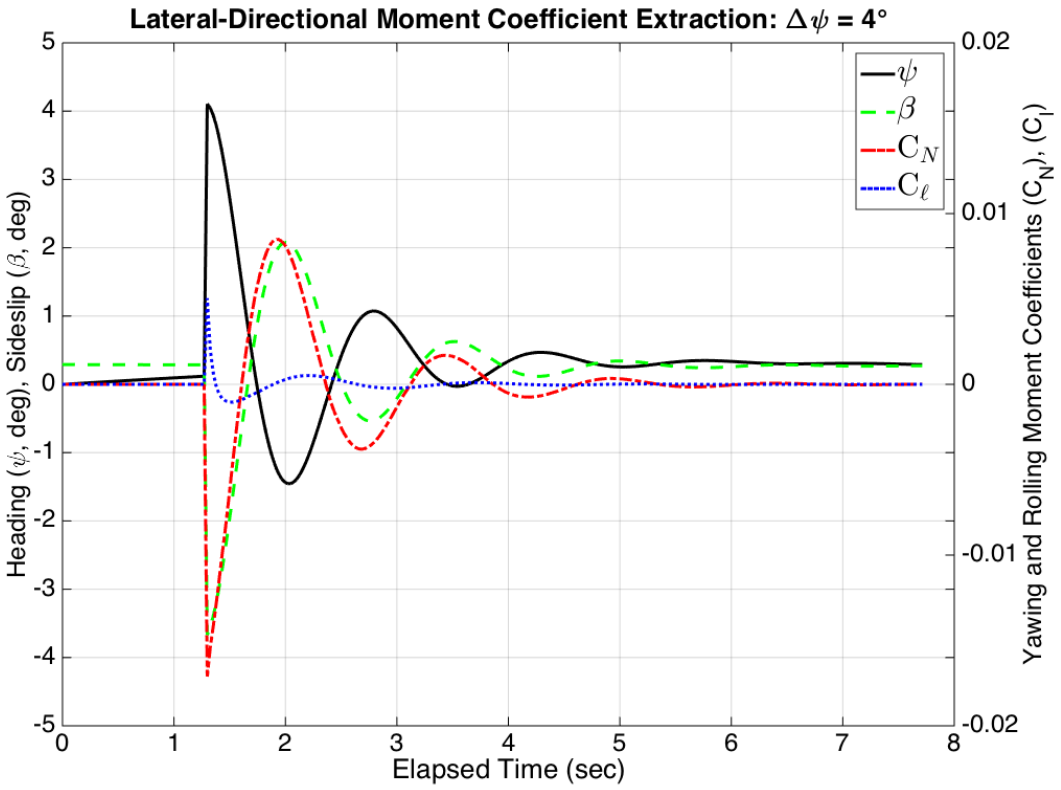

Figure 15: Cessna 172SP time response to impulse heading change

Twelve impulse displacements in heading were performed, from $\Delta\psi = -2^{\circ}$ to $\Delta\psi = 4^{\circ}$. The stability derivatives for C_{N_β} and C_{ℓ_β} were estimated using Equations 23 and 24:

$$\frac{\Delta C_N}{\Delta\beta} = C_{N_\beta} = \frac{N}{qSb} \tag{23}$$

$$\frac{\Delta C_\ell}{\Delta\beta} = C_{\ell_\beta} = \frac{\ell}{qSb} \tag{24}$$

The data from the impulse changes was analyzed in MATLAB, where $\Delta\beta$, ΔC_N, and ΔC_ℓ were identified. The results, averaged for each $\Delta\psi$, are detailed on the next page in Table 16.

Table 16: X-Plane lateral-directional stability derivative extraction details

$\Delta\psi$	-2˚	-1˚	1˚	2˚	3˚	4˚
$\frac{\Delta C_N}{\Delta\beta}$	-0.00433	-0.00433	-0.00432	-0.00433	-0.00432	-0.00433
$\frac{\Delta C_\ell}{\Delta\beta}$	0.00128	0.00128	0.00128	0.00128	0.00128	0.00128

The lateral-directional stability derivative calculations were very consistent, with no clear trend in C_{N_β} or C_{ℓ_β} as the magnitude of the $\Delta\psi$ impulse was changed. These values of C_{N_β} or C_{ℓ_β} are of expected sign and are indicative of the aircraft's yaw and roll stability. Given the consistency of the lateral-directional stability results, they were averaged together for all $\Delta\psi$. The final results are presented in Table 17 below.

Table 17: Final extracted lateral-directional stability parameters

C_{N_β} (deg^{-1})	0.00432
C_{ℓ_β} (deg^{-1})	-0.00128

2.4 Data Comparison (X-Plane 10 vs. Empirical)

2.4.1 Longitudinal Data

The longitudinal stability derivatives extracted from the Cessna 172 model in X-Plane 10 compare favorably to empirical calculations. Overall, all parameters are of correct sign and order of magnitude. The calculated and extracted longitudinal stability derivatives are summarized in Table 18 below.

Table 18: Longitudinal stability derivatives comparison

Source	C_{L_α}	C_{M_α}	$C_{L_{\delta F}}$	$C_{M_{\delta F}}$	$C_{L_{\delta E}}$	$C_{M_{\delta E}}$
Empirical	0.0884	-0.0256	0.0151	-0.00394	0.00613	-0.0188
X-Plane	0.0804	-0.0433	0.0229	-0.00705	0.00850	-0.0377

Note: all terms are in deg^{-1}

X-Plane's basic lift curve slope agrees very well with empirical predictions, as shown in Figure 16. The pitching moment curve slope, an indicator of aircraft's stability, is significantly more negative (more stable) in X-Plane than in empirical calculations.

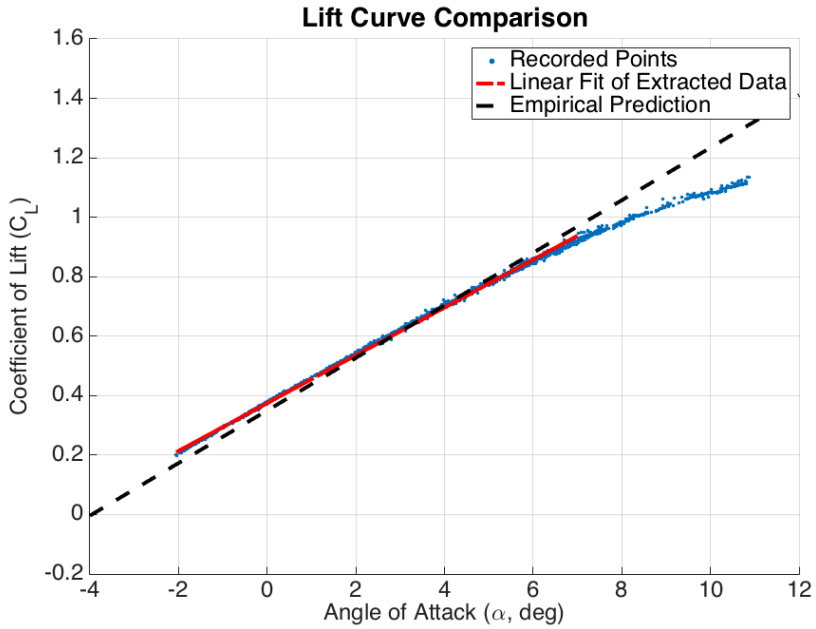

Figure 16: X-Plane and empirical lift curve comparison

For the flap increment terms $C_{L_{\delta F}}$ and $C_{M_{\delta F}}$, X-Plane's increase in moment and lift increments is not surprising. In the empirical calculations, the flaps are treated as plain flaps; in real life, the flaps are slotted with some small Fowler motion. The Cessna 172 model creators may have adjusted the flap coefficient terms based on more accurate knowledge of how the aircraft performs.

The elevator coefficient increment terms $C_{L_{\delta E}}$ and $C_{M_{\delta E}}$ show some of the largest differences between empirical calculations and X-Plane extractions. The exact cause of these differences is not known, but the elevator acts more effectively in X-Plane than what the geometry-based calculations would predict. It is speculated that the propeller

slipstream (and thus, thrust effects) model in X-Plane may contribute to the increased elevator effectiveness. An increase in elevator effectiveness also would increase the magnitude of C_{M_α}. Alternatively, the location of the center of gravity could also make the aircraft appear more or less stable. If interpreted incorrectly during the equivalent geometry process, x_{cg} could have both made the aircraft appear less stable and the elevator less effective.

It should be reiterated that thrust effects were not considered in DATCOM calculations, but are presumably modeled in X-Plane's flight model. With the centerline of thrust at the front of the aircraft and below the center of gravity, adding thrust effects to the Cessna 172 would be destabilizing (moving the neutral point forward). However, since the propeller is in line with the horizontal tail, an increase in dynamic pressure could result in η_{HT} greater than unity, offering a stabilizing effect. The net result of thrust effects was not estimated, but it is not expected to fully account for differences between empirical estimations and X-Plane flight tests.

2.4.2 Lateral-Directional Data

The lateral-directional derivatives C_{N_β} and C_{ℓ_β} are presented in Table 19 below.

Table 19: Lateral-directional stability parameter comparison

Derivative	X-Plane 10	Empirical
C_{N_β} (deg^{-1})	0.00432	0.00120
C_{ℓ_β} (deg^{-1})	-0.00128	-0.00029

While the differences between the X-Plane extractions and empirical calculations are quite large in terms of percentage, all terms are indicative of static lateral-directional

stability. The empirical terms are approximately 25% the magnitude of the X-Plane derivatives. Since the vertical tail is the primary contributor in these sideslip derivatives, this difference may indicate that X-Plane may be treating the vertical tail as more effective than would be expected. This is not all that surprising, however, given the way that X-Plane's vertical tail is constructed in the flight model - including a nearly 50% increase in surface area when compared to equivalent geometry methods. As mentioned in Section 2.2.6, Daniel Raymer estimates the C_{N_β} value of a Cessna 182 as 0.0013 deg^{-1}. This value is only 8% more than the estimated C_{N_β} that was derived from calculations based on equivalent geometry of a Cessna 172. Given this information, it appears that the tail surfaces, both horizontal and vertical, are more effective in X-Plane than in real life. The most important aspect, however, is the yaw and roll stability that the aircraft exhibits in X-Plane's flight model.

Chapter 3: Warning System Development

3.1 Warning System Philosophy

This research set out to design a warning system that gave a pilot a constant-time warning. Other warning systems use margins such as airspeed and angle of attack (AoA), but do not directly consider the amount of time left before a loss of control event occurs. Indirectly, these methods could increase their time margin by increasing their physical margin. However, increasing the physical margin may result in unnecessary and distracting warnings.

As an example, consider a pilot approaching stall with a traditional stall horn warning system. In practice, the stall horn warning system is based off of the aircraft's angle of attack. If a pilot reduces power in straight-and-level flight while holding altitude, the approach to the critical AoA can be relatively slow. However, if a pilot is already near the warning threshold and makes a sharp turn toward final approach of a runway, an increase in load factor may quickly put him into an accelerated stall. The time between hearing the warning and the aircraft actually entering stall can be drastically different in these two cases. Increasing the AoA margin may result in distracting and unnecessary warnings in the first case, but potentially lifesaving reaction time in the second.

An electronic warning system that considers the physical state of an aircraft may be able to account for how quickly the aircraft is approaching an LoC event. The system

would then be able to issue a warning to the pilot based on how much time it expects the pilot will have left to take preventative action. The warning time threshold, t_{warn}, could be changed when an optimum amount of warning time is found. The logic behind issuing an LoC warning would answer the question: "If the aircraft continues to do what it is doing now, in t_{warn} seconds, is there great potential that the pilot could lose control of the aircraft?" The fundamental methods of such a warning system are explored in the following sections as a proof-of-concept.

3.2 Warning System Technique

A simple kinematic equation was used as the basis of the warning system:

$$x = x_0 + \frac{dx}{dt}(t) + \frac{1}{2}\frac{d^2x}{dt^2}(t^2) \tag{25}$$

A similar equation could be found in any elementary physics textbook, where the constant acceleration, one-dimensional motion of an object is described by initial position (x_0), velocity (v), acceleration (a), and position (x) at some time (t):

$$x = x_0 + vt + \frac{1}{2}at^2 \tag{26}$$

Fortunately, "x" could be replaced by any aircraft state parameter. A few suggested parameters are explored in the following sections.

An electronic warning system, if properly equipped, would know the current state (x_0) of some parameter x. With a time history of an aircraft state parameter, the system could calculate the first derivative ("velocity" or rate of change) of the parameter, as well as the second derivative ("acceleration") and have a second-order prediction of where x will be after some time t_{warn}. If that prediction exceeds some maximum (or minimum)

threshold value x_{max}, then a warning would be issued. This concept is illustrated with Equation 27 below.

$$x_0 + \frac{dx}{dt}(t_{warn}) + \frac{1}{2}\frac{d^2x}{dt^2}({t_{warn}}^2) \geq x_{max} \tag{27}$$

It is stressed that this is only one approach and implementation of a warning system. Other methods of prediction and estimation could be used to produce loss of control warnings. The author originally attempted to use a first-order prediction method, but it yielded unsatisfactory results (false warnings and unsatisfactory warning times). Certainly, higher-order estimations of the aircraft's motion could be used, but at the increased cost of practicality and computation time. A balance of prediction complexity and computation time must be used to develop a practical warning system.

3.3 Longitudinal Warnings

3.3.1 Coefficient of Lift

A potential for severe loss of control occurs when an aircraft stalls. A stall occurs when the aircraft's wing(s) exceed a certain angle of attack (α) called the critical angle of attack (α_{crit}). Corresponding with α_{crit}, $C_{L_{max}}$ is the maximum lift coefficient attainable. Figure 17 on the following page is an example of the relationship between α and C_L. Beyond α_{crit}, the aircraft quickly loses lift (C_L decreases) with increasing α. If one wing of the aircraft stalls before the other (such as in an uncoordinated turn at low speed), the quick yawing and rolling moment can encourage the aircraft to enter an aerodynamic spin. In order to prevent stalls and spins, information about the aircraft's angle of attack or its corresponding lift coefficient must be known.

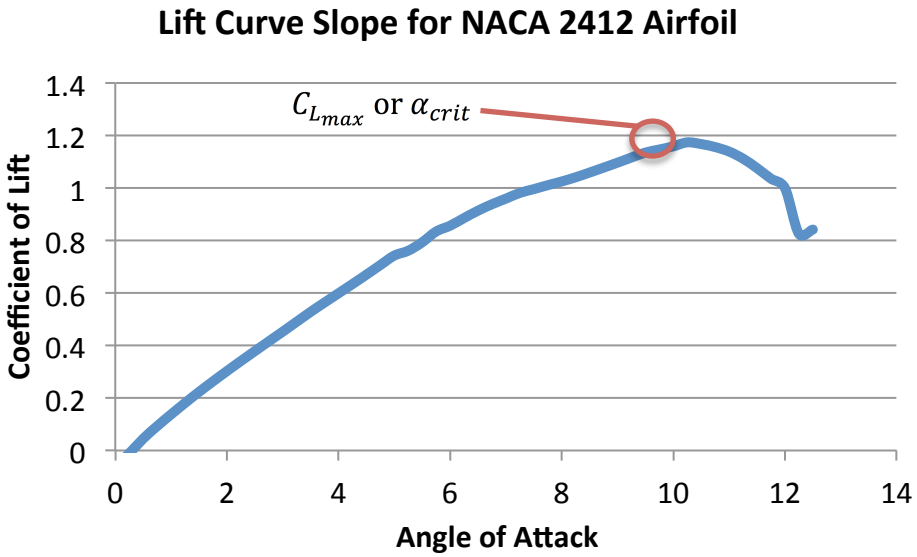

Figure 17: XFOIL lift curve for the NACA 2412 airfoil

An aircraft's lift coefficient, C_L, is given by the standard lift equation:

$$L = \frac{1}{2}\rho v_\infty^2 S C_L \tag{28}$$

This equation can be simplified by defining dynamic pressure (q_∞) as:

$$q_\infty = \frac{1}{2}\rho v_\infty^2 \tag{29}$$

Which results in a new expression for C_L:

$$C_L = \frac{L}{q_\infty S} \tag{30}$$

When an aircraft is in SLUF, the total lift being generated is equal to weight. When the aircraft is in accelerated flight, the lift being generated can be expressed as a load factor, n, times the weight of the aircraft:

$$L = nW \tag{31}$$

Thus, C_L can be expressed as:

$$C_L = \frac{nW}{qS} \tag{32}$$

Equation 32 on the previous page is the basis of the X-Plane implementation as described in this work. This simple expression of C_L makes it attractive for warning system implementation because of the relatively few and uncomplicated sensors it requires to estimate the C_L of the aircraft in real time. A pitot tube, already used on aircraft to determine airspeed, could provide dynamic pressure. Load factor can be easily obtained in flight with an inertial measurement unit (IMU). Weight could be estimated using an initial weight before takeoff and then an average fuel burn of the aircraft.

While the lift coefficient was selected as the basis for stall-type warnings in this research, by no means is the constant-time warning philosophy tied to a specific parameter. It is stressed that other finite difference methods and parameters could be pursued. In a more refined version of the warning system, angle of attack information could be used. Eugene Morelli [18] discusses more robust ways of determining the angle of attack and sideslip with airspeed, angular rates, and translational acceleration; all of these are obtainable with a pitot tube and IMU.

3.3.2 Load Factor

Pilots can find the load limits of an aircraft in the Pilot's Operating Handbook of the aircraft they are flying, but few general aviation aircraft actually include a g-load sensor that the pilot can observe. For the Cessna 172S with flaps up, the POH Normal Category load limits are +3.58g, -1.52g [15]. While the pilot can know the limit for the aircraft, this knowledge does very little good unless it can be used in flight. A g-load warning could be developed with the same concepts as the C_L rate of change warnings discussed in the previous section.

Although a pilot is not likely to meet or exceed the flight load factor limits as listed in the POH in a routine smooth flight, an advanced warning would certainly be helpful in the event that the limits are approached. Flight load limits may be more likely to be approached in turbulence. In this case, an active warning system may keep a pilot away from imminent structural failure. In the event that a pilot's control inputs directly caused load factor exceedance and structural failure resulted, it might be said the pilot should have maintained proper control of the aircraft within its normal flight envelope; this would be considered an LoC event.

3.3.3 Airspeed

Airspeed warnings in general aviation generally focus on stall prevention and thus the lower end of an aircraft's speed capability. An aircraft also has an upper airspeed limit due to structural limitations, often referred to as V_{NE} or the "never exceed" airspeed. While many GA aircraft often have a visual indication on the airspeed indicator (see Figure 18 below), there is not necessarily any other aural or visual warning.

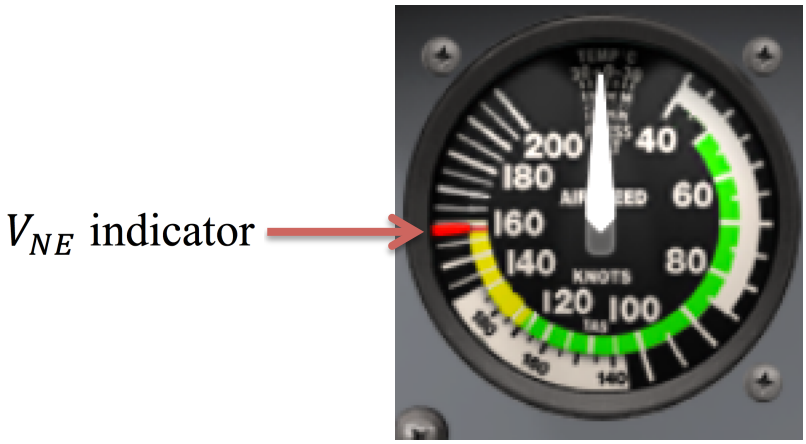

Figure 18: Airspeed indicator from Cessna 172 cockpit

If airspeed is a known parameter, the active warning system and state prediction technique discussed in Section 3.2 would be able to estimate if the aircraft would exceed the "never exceed" (V_{NE}) speed within the given time t_{warn}. It can be argued that a pilot rarely nears such a velocity, but some emergencies, such as an in-flight engine fire, call for a rapid dive to increase airspeed [15]. In such an event, the warning system may prevent a pilot from turning a bad situation into something more deadly.

3.4 Lateral-Directional Warnings

3.4.1 Bank Angle

For most small general aviation aircraft flight, the maximum legal bank angle is considered 60 degrees, unless each occupant is wearing an approved parachuting device [19]. A bank angle warning from an active warning system would potentially warn a pilot when they are about to enter acrobatic flight. Bank angle itself need not be dangerous unless the aircraft has some sort of known operating limitation. Nonetheless, if the warning system uses an inertial measurement unit, it may be readily capable to estimate and issue warnings based on the aircraft's bank angle and roll rate.

3.4.2 Sideslip

The angle of sideslip (β) of an aircraft is as important to the lateral-directional axes as angle of attack is to longitudinal. While it is possible to estimate the sideslip of an aircraft, such as given by Morelli [18], the topic is beyond the scope of this research. An active warning system could warn of high β angles to avoid excessive forces on the aircraft's vertical tail, but such warnings may be unwarranted and distracting to a pilot executing forward slip maneuvers for landing.

A more practical application of sideslip knowledge might be to increase the warning margin (t_{warn}). If an aircraft is approaching stall ($C_{L_{max}}, \alpha_{crit}$) and is flying with a significant β, it is more likely to enter a spin. The knowledge of β could be used to give the pilot a more advanced warning (e.g. increased t_{warn}) due to the extremely dangerous nature of spins.

3.5 X-Plane Plugin Development

The coefficient of lift warning was implemented by creating an X-Plane 10 software plugin. The X-Plane SDK 2.1.3 [20] library was used as an interface to communicate with the proprietary X-Plane 10 flight and graphics model. The code for the warning system plugin was written in the C programming language for compatibility with X-Plane and the X-Plane SDK. The plugin interfaced with a customized Cessna 172SP model that displayed warnings to the "pilot" through a modified cockpit panel.

Plugins in X-Plane run at the mercy of the flight model. Each time a flight model "frame" is calculated, the warning system plugin was called. When activated, the plugin would store the most recent flight data ("real time") and perform calculations and logical evaluations that determined when a warning would be issued. The plugin is capable of storing a user-set amount of historical frames in memory. This historical data is used for calculations that determine when a warning should be issued. A simplified explanation of this process is shown in Figure 19 below.

Figure 19: Warning system process

3.5.1 Method of Communicating Warning

For testing and development purposes, the standard cockpit panel was modified to include a visual warning indicator as shown in Figure 20 below.

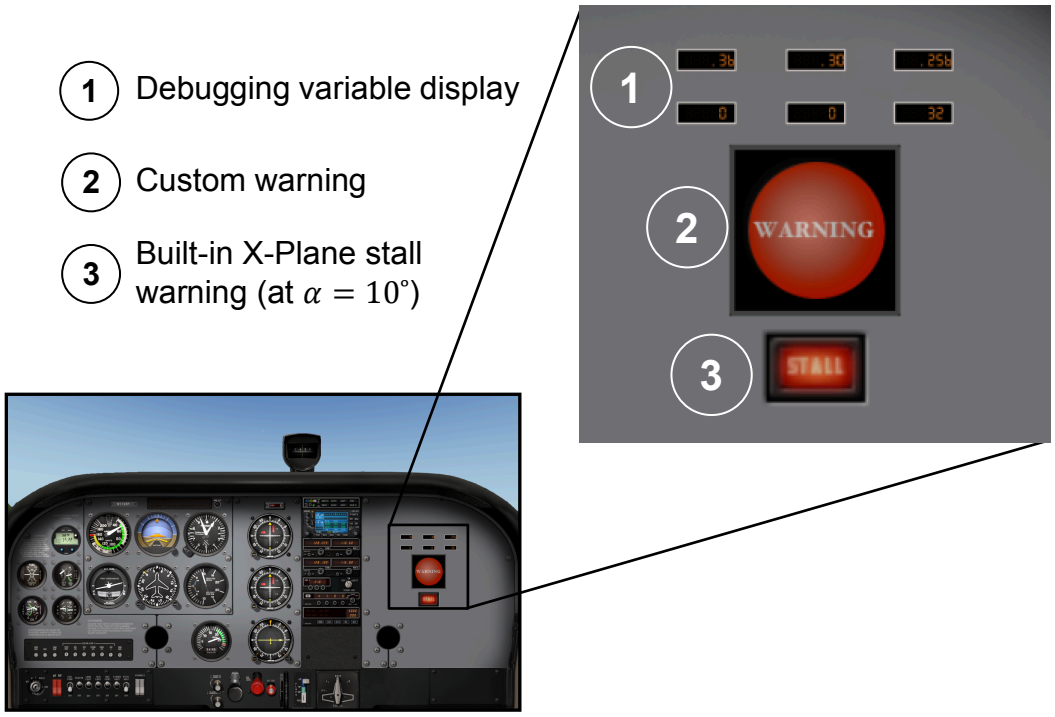

Figure 20: Modified cockpit used in warning system development

Item 1, the two rows of number displays, was used to debug the warning system. Variables that needed to be seen for debugging purposes were displayed in the top row if they were float values and bottom row if they were integers. Item 2 was the visual custom warning alert. It turned bright red as shown in Figure 20 above, and had a darker "off" setting as shown in Figure 21 on the following page. Item 3 was X-Plane's built-in stall warning, which alerted the user when the aircraft's α was greater than 10°. A visual warning (Item 2, Figure 20) was issued to the custom cockpit panel when the real-time calculations of the warning system indicated an alert was required. The warning request

was sent to the cockpit by changing the value of a discrete variable from 0 to 1. This variable was capable of being output by X-Plane so it was directly comparable to the results from the built-in stall warning.

Figure 21: Modified cockpit with warning system off

3.5.2 Calculations

Finite difference methods were employed to find the first and second derivatives of the Coefficient of Lift with respect to time in X-Plane. For the purposes of this discussion, assume that C_L of the aircraft is directly available in X-Plane 10 and no calculations, such as Equation 32 need to be performed. Based on Equation 27 (Section 3.2), the equation below was used to predict the aircraft's C_L after t_{warn} seconds. A warning was issued when it was predicted that C_L was greater than the $C_{L_{warn}}$.

$$C_{L_{RT}} + \frac{dC_L}{dt}(t_{warn}) + \frac{1}{2}\frac{d^2C_L}{dt^2}({t_{warn}}^2) \geq C_{L_{warn}} \tag{33}$$

In the above equation, $C_{L_{RT}}$ is the "real-time" estimated coefficient of lift. A warning was also issued if at any time the estimated $C_{L_{RT}}$ was greater than $C_{L_{warn}}$.

When estimating the derivatives with finite difference methods, nonuniform spacing in time was assumed. X-Plane 10 calculates computational and graphics frames as fast as the computer hardware allows. The time that elapses between each frame is not necessarily constant, so assuming a constant change in time (Δt) from frame to frame would result in less accurate estimations of the derivatives.

First Derivative Method

For calculating $\frac{dC_L}{dt}$, a Lagrange polynomial was used to find a three-point backwards difference (nonuniform spacing) approximation of the second derivative. The original Lagrange polynomial was found using the methods described in Gilat & Subramanium's text [21]:

$$C_L(t) = \frac{(t-t_1)(t-t_2)}{(t_0-t_1)(t_0-t_2)} C_{L_0} + \frac{(t-t_0)(t-t_2)}{(t_1-t_0)(t_1-t_2)} C_{L_1} + \frac{(t-t_0)(t-t_1)}{(t_2-t_0)(t_2-t_1)} C_{L_2} \tag{34}$$

If the first derivative (i.e. $\frac{dC_L}{dt}$) is found and evaluated at x_2, the three-point backward difference for general spacing is given by Equation 35:

$$C_L{}'(t_2) = \frac{t_2-t_1}{(t_0-t_1)(t_0-t_2)} C_{L_0} + \frac{t_2-t_0}{(t_1-t_0)(t_1-t_2)} C_{L_1} + \frac{2t_2-t_0-t_1}{(t_2-x_0)(t_2-t_1)} C_{L_2} \tag{35}$$

where

$$C_{L_2} = C_{L_{RT}} \text{ (real-time } C_L\text{)}$$

$$C_{L_1}, C_{L_0} = \text{time history values of } C_L$$

$$t_2 = \text{current simulator time}$$

$$t_1, t_0 = \text{recorded simulator times corresponding to } C_{L_1}, C_{L_0}$$

Because of X-Plane's inherently discrete calculation model, smoother results in the first derivative calculations can be achieved by considering more than the last three frames in

the simulation. The averaging and weighting process employed for the first derivative is the same as the second derivative method below, but with three terms instead of four.

Second Derivative Method

For calculating $\frac{d^2C_L}{dt^2}$, a Lagrange polynomial was used to find a four-point backwards difference (nonuniform spacing) approximation of the second derivative. The original Lagrange polynomial was found using the methods described in Gilat & Subramanium's text [21]:

$$C_L(t) = \frac{(t-t_1)(t-t_2)(t-t_3)}{(t_0-t_1)(t_0-t_2)(t_0-t_3)}C_{L_0} + \frac{(t-t_0)(t-t_2)(t-t_3)}{(t_1-t_0)(t_1-t_2)(t_1-t_3)}C_{L_1} \tag{36}$$

$$+ \frac{(t-t_0)(t-t_1)(t-t_3)}{(t_2-t_0)(t_2-t_1)(t_2-t_3)}C_{L_2} + \frac{(t-t_0)(t-t_1)(t-t_2)}{(t_3-t_0)(t_3-t_1)(t_3-t_2)}C_{L_3}$$

If the second derivative (i.e. $\frac{d^2f(x)}{dx^2}$) is found and evaluated at x_3, the four-point backward difference for general spacing is given by Equation 37:

$$C_L''^{(t_3)} = \frac{4t_3-2t_1-2t_2}{(t_0-t_1)(t_0-t_2)(t_0-t_3)}C_{L_0} + \tag{37}$$

$$\frac{4t_3-2t_0-2t_2}{(t_1-t_0)(t_1-t_2)(t_1-t_3)}C_{L_1} + \frac{4t_3-2t_0-2t_1}{(t_2-x_0)(t_2-t_1)(t_2-t_3)}C_{L_2} + \frac{6t_3-2t_0-2t_1-2t_2}{(t_3-t_0)(t_3-t_1)(t_3-t_2)}C_{L_3}$$

where

$C_{L_3} = C_{L_{RT}}$ (real-time C_L)

$C_{L_2}, C_{L_1}, C_{L_0}$ = time history values of C_L

t_3 = current simulator time

t_2, t_1, t_0 = recorded simulator times corresponding to $C_{L_2}, C_{L_1}, C_{L_0}$

Because of X-Plane's inherently discrete calculation model (see Section 3.6.4), smoother results in acceleration calculations can be achieved by considering more than the last four frames in the simulation. By averaging a number (N) of C_L data points and weighting the

values based on the time elapsed in the simulator frame(s), 4xN data points can be considered. Using this method, C_{L_3} would be a time-weighted average of the most recent data point and the N-1 previous points. C_{L_2} would be a time-weighted average of the (N+1) frame to (2N-1). This pattern continues until 4xN frames have been considered for the second derivative approximation. For a more graphical illustration of this process, see Figure 22 below, where N=3 is used for the evaluation of 12 recorded C_L values.

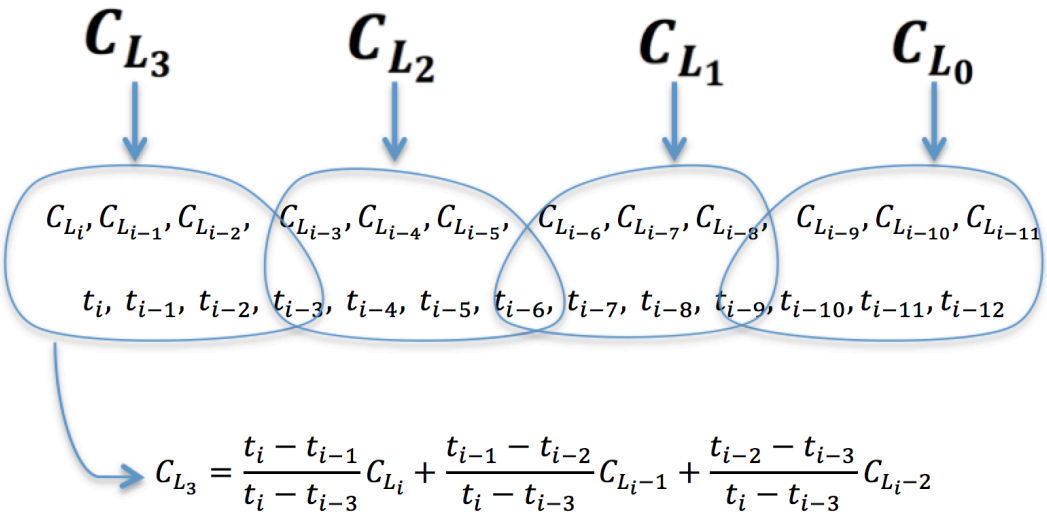

Figure 22: Explanation of averaging for parameter estimation

In the above Figure 22, C_{L_3} corresponds to the real-time $C_{L_{RT}}$ as described in Equation 33 and the parameters $C_{L_2}, C_{L_1}, C_{L_0}$ are the historical data points.

While hypothetically a large number of data points could be considered to determine acceleration, the fewer data points used, the closer the estimation should be to the real-time acceleration. Thus, a balance must be struck between data quality ("smoothness") and data timeliness. A large set of sample points may offer an accurate average acceleration over a time set of 4 or 5 seconds, but the calculated acceleration would not be current enough to issue a time-sensitive warning. Because of this, the

number of frames being considered for any finite difference calculation should depend on the time spacing between data points and how quickly the hardware is able to process the calculations.

3.6 Results

3.6.1 System Setup

X-Plane 10.32 was executed on an Apple MacBook Pro with Mac OS X 10.10, a 2.3 GHz Intel® Core i7™, 16 GB RAM, and an NVIDIA® GeForce GT 750 2GB graphics card. Graphical frames were calculated at 20-40 frames per second, with 30 frames per second being typical. X-Plane 10's Flight Model calculations were set to calculate twice per graphics frame, but software plugins can only run in sync with graphical frames. Thus, it was indirectly possible for X-Plane to render frames faster or slower based on how many graphics options were turned on.

The warning system plugin was set to use a $C_{L_{warn}}$ of 1.08. For data comparison purposes, this $C_{L_{warn}}$ approximately corresponds to the $\alpha_{warn} = 10^{\circ}$ for the stall horn in X-Plane's Cessna 172SP model. The first and second derivatives were set to use the last 9 and 8 frames for calculations (see Figure 22). The warning margin, t_{warn}, was set to 2.2 seconds with an expected efficacy of 2.0 seconds of warning before loss of control due to error-checking processes used to prevent false warnings. While t_{warn} could be set to any value, 2.2 seconds yielded acceptable results in testing. Further study should be considered to determine optimum time for a pilot to respond to a loss of control event.

3.6.2 Pull Up from Straight and Level Flight

To demonstrate the fundamentals of the C_L-based "constant-time" warning system, flight tests were performed in X-Plane. The Cessna 172SP was trimmed in SLUF at approximately 2,000 ft MSL and 80 KIAS. While targeting wings-level flight, the control yoke was pulled back until at least the beginning of a stall. Two types of flight tests, one with a slower and the other a more rapid pull on the control yoke, were performed for data analysis.

For the first type flight test, the control yoke was pulled back slowly from SLUF trimmed state until stall occurred. A time history of α, C_L, and the activation of the built-in stall warning and the new plugin-based warning system is show in Figure 23 below.

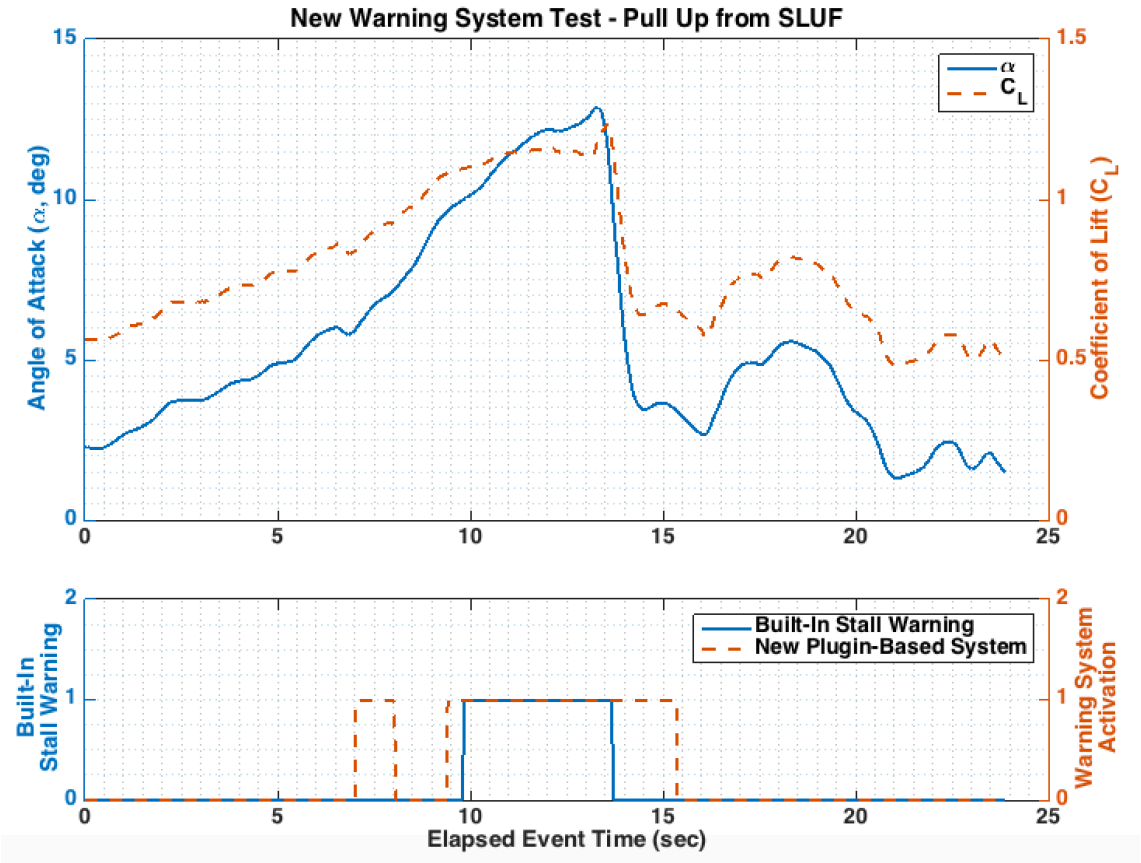

Figure 23: Time history of slow SLUF pull up warning test

For a more complete time history that includes other aircraft state terms, see Figure C-1 in Appendix C. In Figure 23, the warning system plot indicates whether or not a warning was being issued (a value of 1) or was not being issued (a value of 0). The warning that begins at about 6.5 seconds is a false warning and is ignored for this discussion (see Section 3.6.4).

For this slow pull up from SLUF, the new warning system activates 0.43 seconds before the built-in stall warning of $\alpha_{warn} = 10^{\circ}$ and about 2.5 seconds before stall. For the purposes of this discussion, stall occurs where an increase in α no longer shows an increase in C_L. While the system is meeting an expected warning margin (t_{warn}) of 2.0 seconds before stall, it technically was set up to issue a warning t_{warn} seconds before $C_{L_{warn}}$ was reached. Therefore, while an improvement is shown when compared to the built-in stall warning, the new "constant-time" warning system did not offer quite as much warning as expected for a slow pull up from SLUF. Slightly more favorable results are seen in Figure 24 on the following page, a time history of a more rapid pull up from SLUF conditions. For a more complete time history with additional parameters, see Figure C-2 in Appendix C.

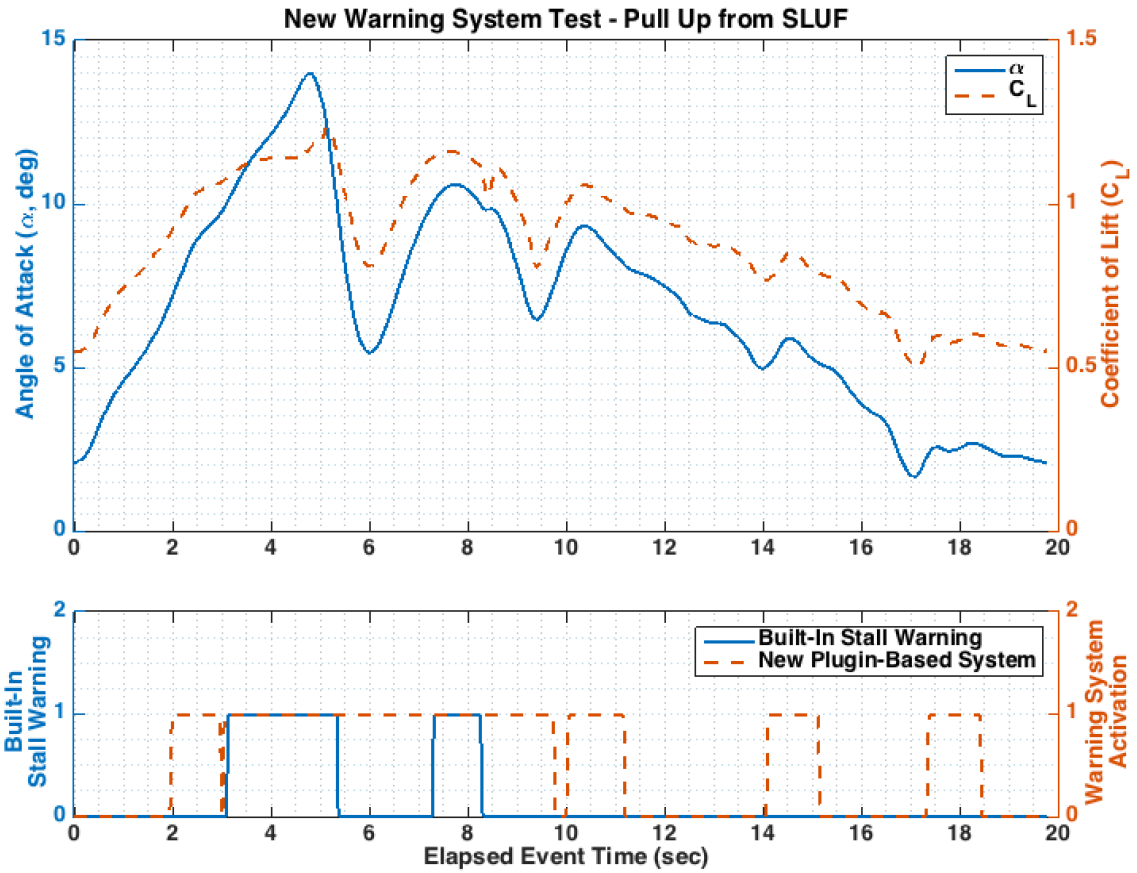

Figure 24: Time history of fast SLUF pull up warning test

For this quick pull up from SLUF, the new warning system activates 1.15 seconds before the built-in stall warning of $\alpha_{warn} = 10^{\circ}$ and about 2.3 seconds before stall. Again, the system is meeting the expected t_{warn} before stall, but not quite giving as advanced of a warning as expected. Nonetheless, a clear improvement is shown when compared to the built-in stall warning system.

Also interesting to note is the near-constant warning activation during the attempted recovery from stall. Considering the shape of the C_L curve post-stall, it is reasonable that the warning system might expect the predicted C_L after t_{warn} seconds to

be at or above $C_{L_{warn}}$. This is because after pushing the nose down for recovery from the stall, the angle of attack is then rapidly increased at least twice.

3.6.3 "Turn to Final" Simulation

In a more practical application, the C_L-based "constant-time" warning system was flight-tested on a simulated "Turn to Final." Typically, at this stage of flight, the flaps and gear are extended while the aircraft makes a turn to final approach of the runway. In attempt to line up with the runway, the pilot may pull on the control column in an attempt to maintain altitude and tighten the turn. It is a very high-workload situation in flight, so an active warning system can be very useful for keeping the pilot away from Loss of Control.

To simulate a turn to final approach, the aircraft was trimmed in SLUF (flaps up) at approximately 2,000 ft MSL and 80 KIAS. Throttle was then reduced to initiate a descent. Although the speed and flaps up configuration are not exactly what one might expect for an approach to landing in a Cessna 172, emergency conditions may preclude flap usage. With a steady descent established, the aircraft was rolled to the left and the yoke was pulled to increase load factor. Zero sideslip and 45˚ left bank were targeted during the maneuver. Figure 25 on the next page shows the time history of one such recorded maneuver. For a more complete time history with additional parameters, see Figure C-3 in Appendix C.

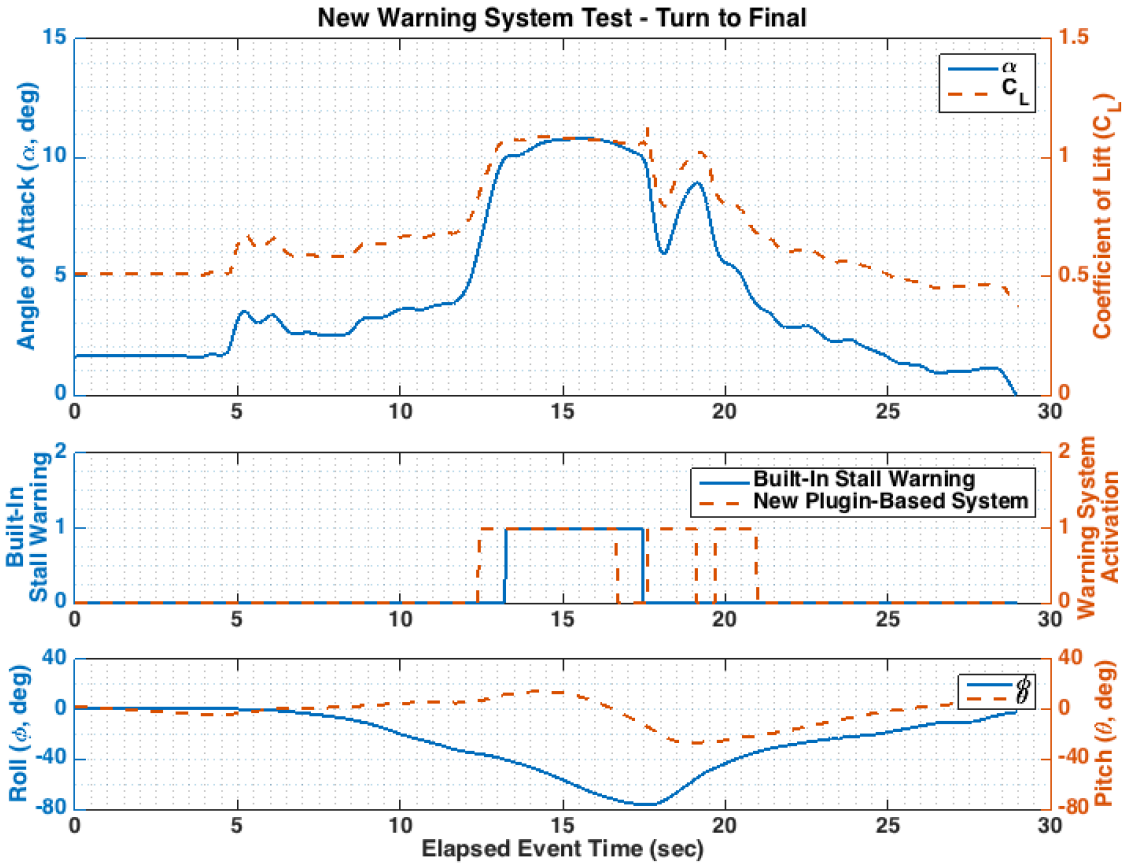

Figure 25: Time history of "Turn to Final" warning test

For this simulated turn to final, the new warning system activates 0.83 seconds before the built-in stall warning and 2 seconds before stall. As expected, banked turns with increased load factor are no hindrance to the warning system's C_L-based operation. Again in the above figure, the new warning system issues alerts during the rapid α changes during the recovery from the stall. While such operation could be considered a "false warning," it could also be a quite useful improvement in preventing secondary stalls.

3.6.4 False Warnings

X-Plane 10 uses an inherently discrete mathematical model of continuous-time physics. Because of its inherently discrete calculations, frame-to-frame changes sometimes appear larger and more dramatic than they would in a continuous time curve. Conversely, if an aircraft is relatively in SLUF, extremely tiny changes in a variable that has been relatively steady can occasionally result in a higher than expected calculated rate of change. Both of these situations can cause false warnings in the X-Plane based plugin warning system, so error-checking has been included in plugin source code. The error-checking and debugging techniques, which were implemented during the data collection process, include:

1. Only begin issue a warning if the calculations from the last four frames (approximately 0.15 seconds) have indicated a warning was needed.
2. Do not begin to issue a warning if the current C_L is less than one-half the maximum value.
3. Keep the cockpit warning light on for at least 1 second after the last command to issue a warning to the cockpit (makes false warnings visually easier to identify).

Although false warnings occasionally are still present (especially with very rapid accelerations/turbulence), the quality of the warnings has improved.

Chapter 4: Conclusions and Future Work

4.1 Thoughts on Practical Implementation

The warning system methods described in this work have potential for cost-effective implementation into existing and future small GA aircraft. Many newer aircraft have Electronic Flight Instrument Systems with digital displays. These EFIS (Glass Cockpits) offer a vast array of information that could be used in an active constant-time warning system. With aircraft physical state and configuration information already available in a digital format, the implementation of an active warning system would be as simple as writing compatible source code similar to that demonstrated in this research. The warning system would be completed with aural and visual warnings installed in the cockpit.

For older aircraft, the cost and relative ease of installation of the proposed warning system would depend on the complexity of the system. For instance, a system that adjusts warning parameters based on aircraft configuration would need to know the position of the gear and flaps – information that is likely not in a digital format. At a minimum, the proposed warning methods would require a digital hardware package complete with sensors, processor, aural/visual warning alerts, and a power source.

It is the author's opinion that a simpler C_L or α based warning system would be most successful for implementation in older analog-cockpit aircraft. A system with more

warning features (complexity) would have more success in current EFIS-equipped aircraft. Regardless of the exact implementation, the nonuniform spacing finite difference methods employed in the X-Plane plugin apply well to real hardware usage. With precise real-time clock hardware, the code would be able to adapt for changes in runtime between loops.

For any aircraft, the limiting parameters of the system (such as $C_{L_{max}}$ and V_{NE}) must be customized to the aircraft's flight characteristics. Extensive flight testing and evaluation should be performed before it would be considered "flight-ready."

4.2 Conclusions

4.2.1 X-Plane Flight Model

The X-Plane Cessna 172 flight model compares favorably with empirical calculations of flight characteristics. In longitudinal and lateral-directional cases, the data extractions from X-Plane indicate a higher degree of static stability than the actual aircraft is expected to possess. It is speculated that X-Plane may model airflow in a way that increases the effectiveness of empennage surfaces beyond their expected capabilities. Since equivalent geometry and empirical formulae were used to estimate the performance, errors should be expected from this process. Using actual Cessna 172 flight test time history data could offer improved comparisons. Unfortunately, using real flight test data for the development of a new warning system method would greatly increase the cost, especially if each aircraft would need a full flight test evaluation before installation.

Despite the minor differences between X-Plane and empirical calculations, X-Plane's flight model is considered acceptable for the development of an active warning

system. Static stability characteristics are of expected sign and magnitude and offer a realistic flight experience in the simulator. When using X-Plane for warning system development, results that are comparable to real-world flight dynamics are expected.

4.2.2 Warning Method

The foundation of a constant-time warning system has been created using a flight simulator that has been customized with software plugins and modified cockpit panels. As demonstrated in this proof of concept, the constant-time warning system considers the aircraft's current state of the lift coefficient and predicts whether a loss of control event (exceeding the maximum lift coefficient) is likely to occur within a time warning margin. Significant warning time improvements (more than one second) to X-Plane's built-in angle of attack stall warning have been observed, but a consistent "constant-time" warning has not yet been achieved. In practice, the best improvements come from rapid approaches to Loss of Control events, where existing physical margins may not provide enough time for the pilot to react safely.

The potential effects of an improved LoC warning method are noteworthy, as Loss of Control is the single largest contributor to GA accidents and fatalities. The constant-time warning method should be extended to include other flight parameters to improve its LoC event recognition and reduce false warnings. Additionally, the system could be programmed to adjust its time warning margin based on the severity of the expected LoC event (e.g. a stall at high sideslip is more likely to lead to a spin, so additional warning margin could be used).

4.3 Future Work

The successful results of the X-Plane Flight Model Cessna 172SP comparison to empirical data encourage the continued development of improved Loss of Control warning systems on X-Plane 10. The stall warning concepts that were applied in the C_L implementation should be extended to other flight envelope excursions, such as the parameters given in Sections 3.3 and 3.4, using rate of change and finite difference methods as described in Sections 3.2 and 3.5.2. Overspeed, load factor, and bank angle warnings may prove to be useful to a general aviation pilot.

For further refinement, many flight conditions should be evaluated and the warning system should compensate for the aircraft's configuration. Additional sensors would be needed for configuration parameters such as flap extension, and gear position. With such added capability, warnings could then be issued for gear and flap overspeed, and warnings based on α and C_L would better adjust for landing and takeoff configurations.

A stated goal of this research was to provide better LoC warnings that would not require the pilot to be looking inside the cockpit. Additional warnings, including enhanced visual and aural warnings, could be added to the simulated cockpit panel in X-Plane. It is not assumed that the simulated warning light in Figure 20 is not a sufficient notification. Enhanced aural warnings would be able to warn a pilot not just of a potential loss of control, but also hint of what is causing the alarm. For example, a warning system might say "Push Forward!" to lower the nose in the case of excessive angle of attack or positive load factor.

After a complete set of warning features have been thoroughly tested and debugged in X-Plane, the opinion of general aviation pilots (especially flight instructors and private pilots) should be sought. Pilot opinions and evaluation of the warning system would provide needed feedback before the warning system is transferred to physical hardware for flight evaluation. Additionally, multiple piloted test flights on the simulator would be useful in determining a warning time margin required for loss of control prevention.

References

[1] Aircraft Owners and Pilots Association. What is General Aviation. [Online]. http://www.aopa.org/letsgoflying/ready/steps/whatis.html

[2] National Transportation Safety Board. (2014, January) Summary of US Civil Aviation Accidents for Calendar Year 2012. [Online]. http://www.ntsb.gov/investigations/data/Pages/2012%20Aviation%20Accidents%20Summary.aspx

[3] Rich Stowell, "Pilot-in-control," *FAA Safety Briefing*, vol. 51, no. 2, March/April 2012.

[4] Daryl Smith, *Controlled Flight Into Terrain (CFIT/CFTT)*. New York, NY: McGraw-Hill, 2001.

[5] Richard L. Collins, *Air Crashes*. New York, NY: Macmillan, 1986.

[6] Federal Aviation Administration, *Pilot's Handbook of Aeronautical Knowledge*. Oklahoma City, OK: U.S. Department of Transportation, 2008, FAA-H-8083-25A.

[7] Stall Warning, 14 CFR 23.207 , 1996.

[8] Advanced Flight Systems, Inc. Advanced Angle-of-Attack. [Online]. https://www.advanced-flight-systems.com/Products/AOA/aoa.html

[9] Federal Aviation Administration, "Installation, training, and use of non-required/supplemental angle-of-attack (AOA) based systems for general aviation (GA) airplanes ," Flight Standards Service, Federal Aviation Administration, Washington, DC, InFO 14010, 2014.

[10] Noel J. Duerksen, John C. Johnson, and Justin S. Williams, "Envelope protection for mechanically-controlled aircraft," Grant US8195346 B1, January 21, 2009.

[11] Laminar Research. (2014) X-Plane 10 Global. [Online]. www.x-plane.com

[12] Laminar Research. Appendix A: How X-Plane Works. [Online]. http://wiki.x-plane.com/Appendix_A:_How_X-Plane_Works

[13] Jan Roskam, *Methods for Estimating Stability and Control Derivatives of Conventional Subsonic Airplanes*. Lawrence, KS, United States: Published by the Author, 1971.

[14] Daniel P. Raymer, *Aircraft Design: A Conceptual Approach*, 5th ed. Reston, VA: American Institute of Aeronautics and Astronautics, 2012.

[15] Cessna Aircraft Company, Pilot's Operating Handbook: Model 172S Nav III , October 2006.

[16] Ira H. Abbott, Albert E. von Doenhoff, and Louis S. Stivers, Jr., "Summary of airfoil data," National Advisory Committee for Aeronautics, Langley Field, VA, Report 824. 1945.

[17] X-Plane SDK Community. (2014, May) X-Plane SDK Wiki. [Online]. http://www.xsquawkbox.net/xpsdk/mediawiki/MovingThePlane

[18] Eugene A. Morelli, "Real-time aerodynamic parameter estimation without air flow angle measurements," *Journal of Aircraft*, vol. 49, no. 4, pp. 1064-1074, July-August 2012.

[19] Federal Aviation Administration, 14 CFR 91.307 - Parachutes and Parachuting.

[20] X-Plane SDK Team. X-Plane Software Development Kit - Main Page. [Online]. http://www.xsquawkbox.net/xpsdk/mediawiki/

[21] Amos Gilat and Vish Subramaniam, *Numerical Methods for Engineers and Scientists*, 3rd ed. United States of America: Wiley, 2013.

Appendix A: Additional General Aviation Statistics

Table A-1: Detailed NTSB general aviation accident data from calendar year 2012 **[2]**

General Aviation Accident Aircraft by Flight Purpose and Aircraft Category, 2012							
Purpose of Flight	**Fixed-Wing**	**Helicopter**	**Glider**	**Balloon**	**Other**	**Unknown**	**Total**
Personal	887	44	23	5	29	0	988
Instructional	172	29	6	0	1	0	208
Aerial Application	53	14	0	0	0	0	67
Business	22	7	0	1	0	1	31
Positioning	21	10	0	0	0	0	31
Public Use	11	14	0	0	0	0	25
Other Work Use	8	8	0	8	0	0	24
Aerial Observation	11	7	0	0	0	0	18
Flight Test	11	2	0	0	3	1	17
External Load	0	12	0	0	0	0	12
Executive/Corporate	7	4	0	0	0	0	11
Ferry	8	3	0	0	0	0	11
Skydiving	10	0	0	1	0	0	11
Banner Tow	7	0	0	0	0	0	7
Air Race/Show	6	0	0	1	0	0	7
Glider Tow	1	0	1	0	0	0	2
Air Drop	2	0	0	0	0	0	2
Fire Fighting	0	1	0	0	0	0	1
Unknown	13	0	0	0	0	1	14
Total	1250	155	30	16	33	3	1487

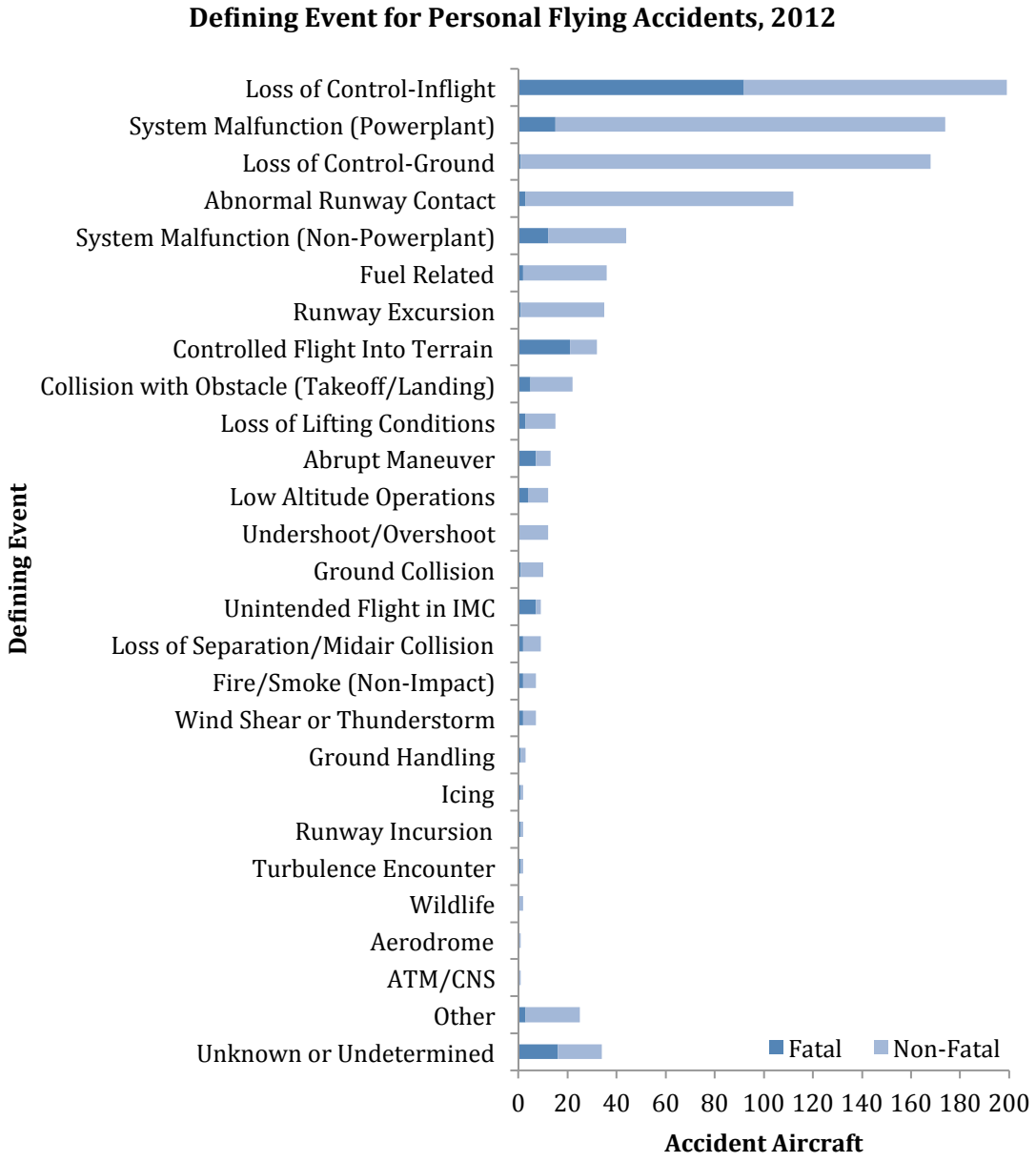

Figure A-1: Full defining event data for personal flying accidents in 2012 **[2]**

Appendix B: X-Plane Wing Model

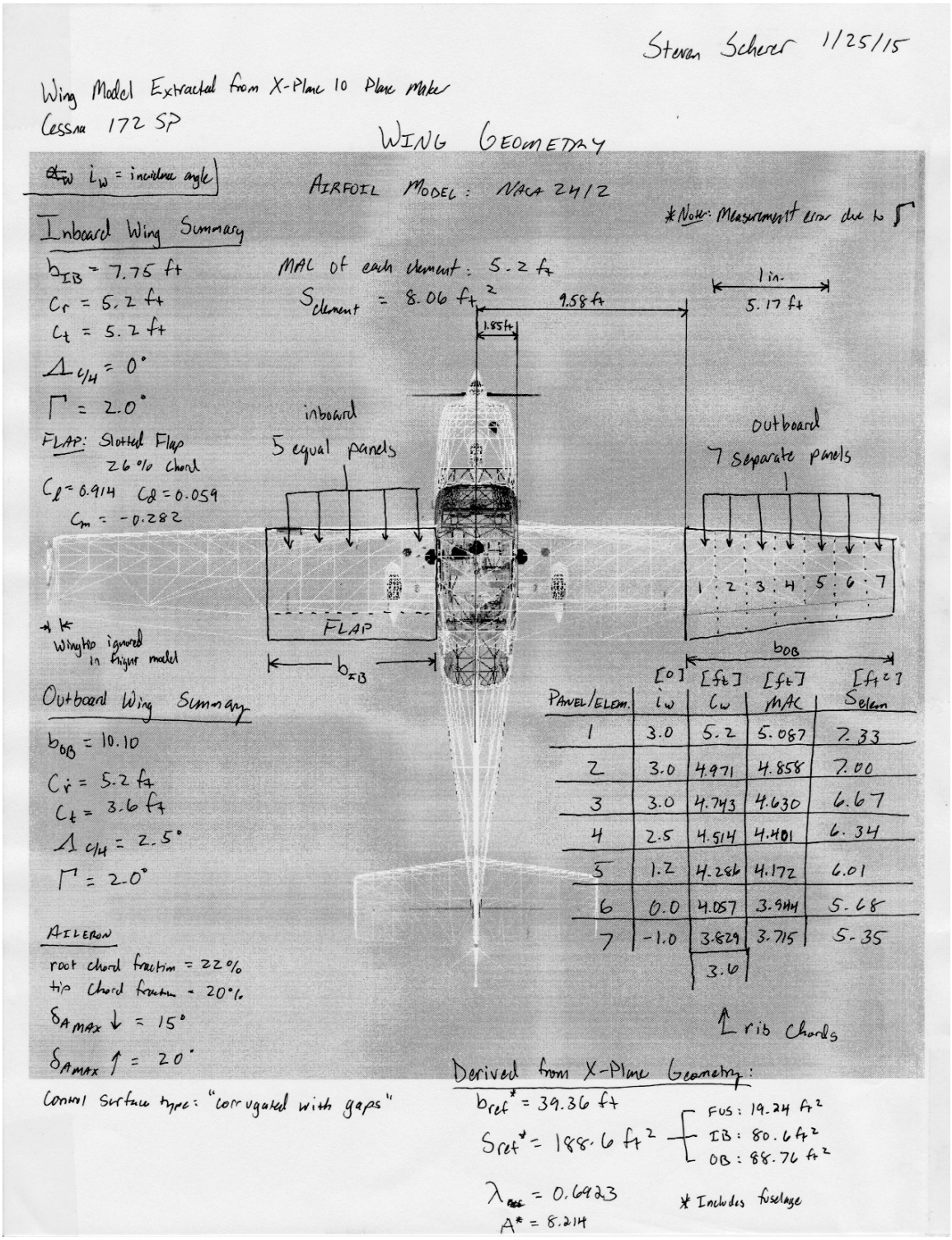

Panel/Elem.	[°] i_w	[ft] C_w	[ft] MAC	[ft²] S_{elem}
1	3.0	5.2	5.087	7.33
2	3.0	4.971	4.858	7.00
3	3.0	4.743	4.630	6.67
4	2.5	4.514	4.401	6.34
5	1.2	4.286	4.172	6.01
6	0.0	4.057	3.944	5.68
7	-1.0	3.829	3.715	5.35
		3.6		

Figure B-1: X-Plane wing model details

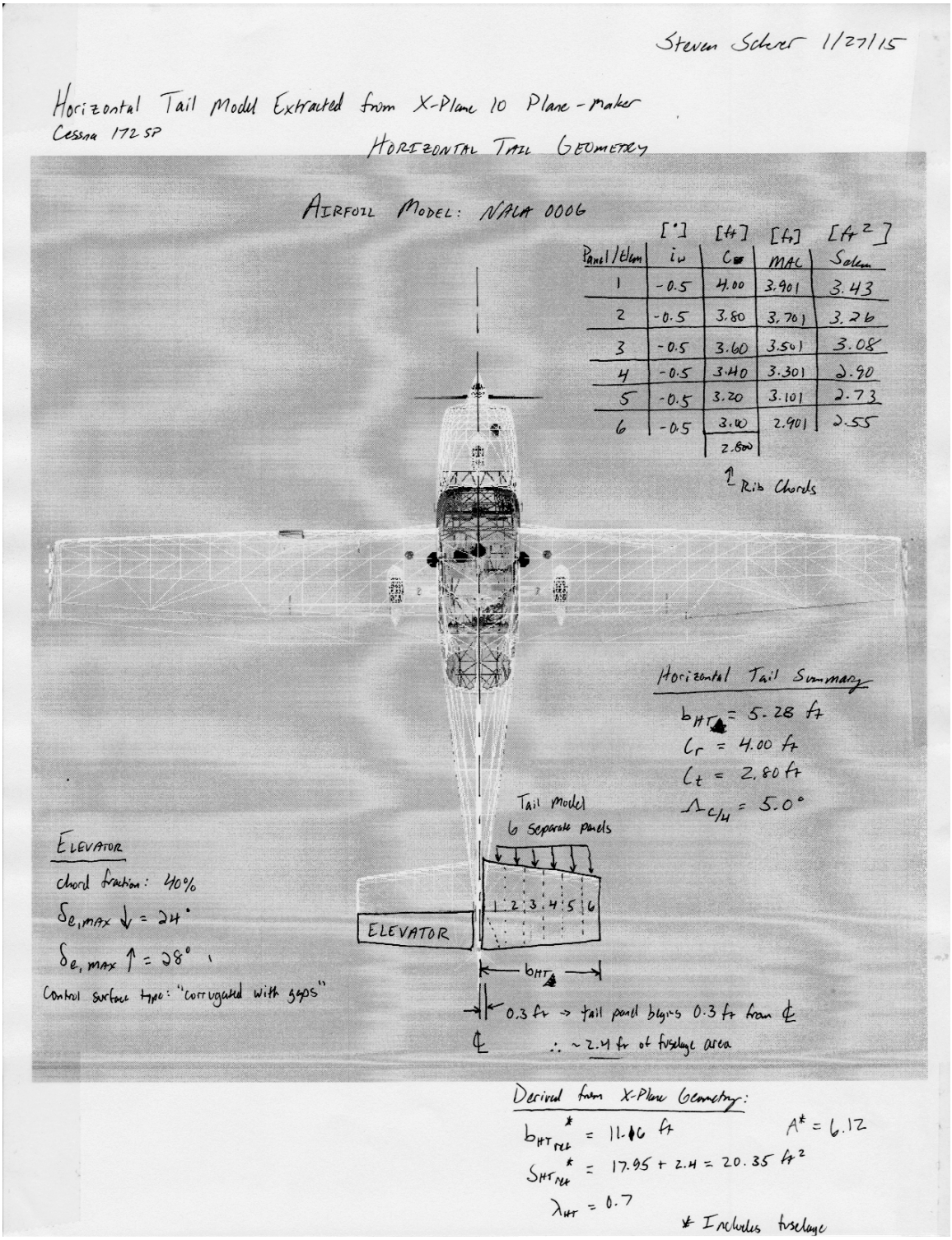

Figure B-2: X-Plane horizontal tail model details

Figure B-3: X-Plane vertical tail model details

Appendix C: Warning System Data

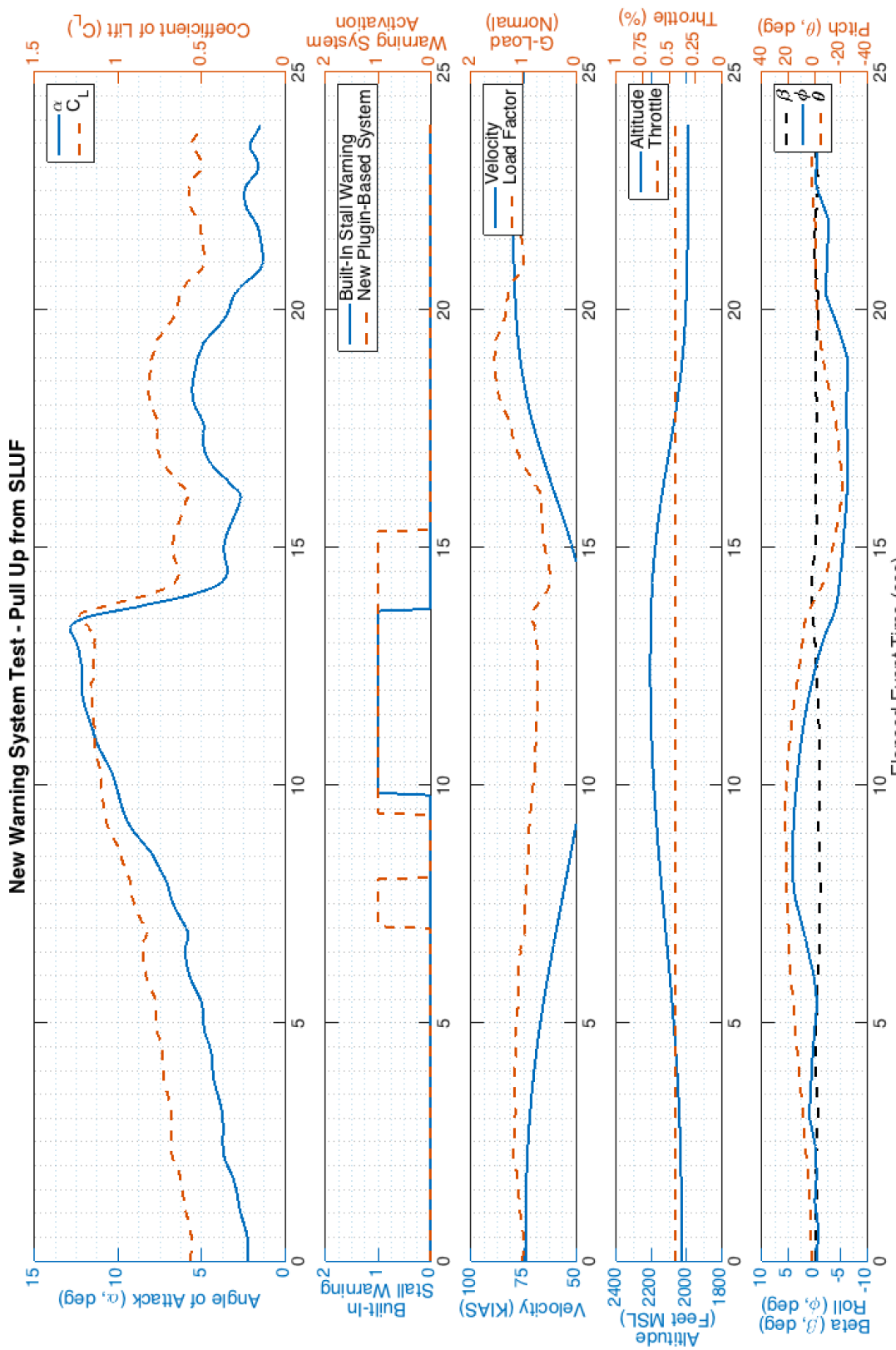

Figure C-1: Detailed time history data of slow SLUF pull up warning test

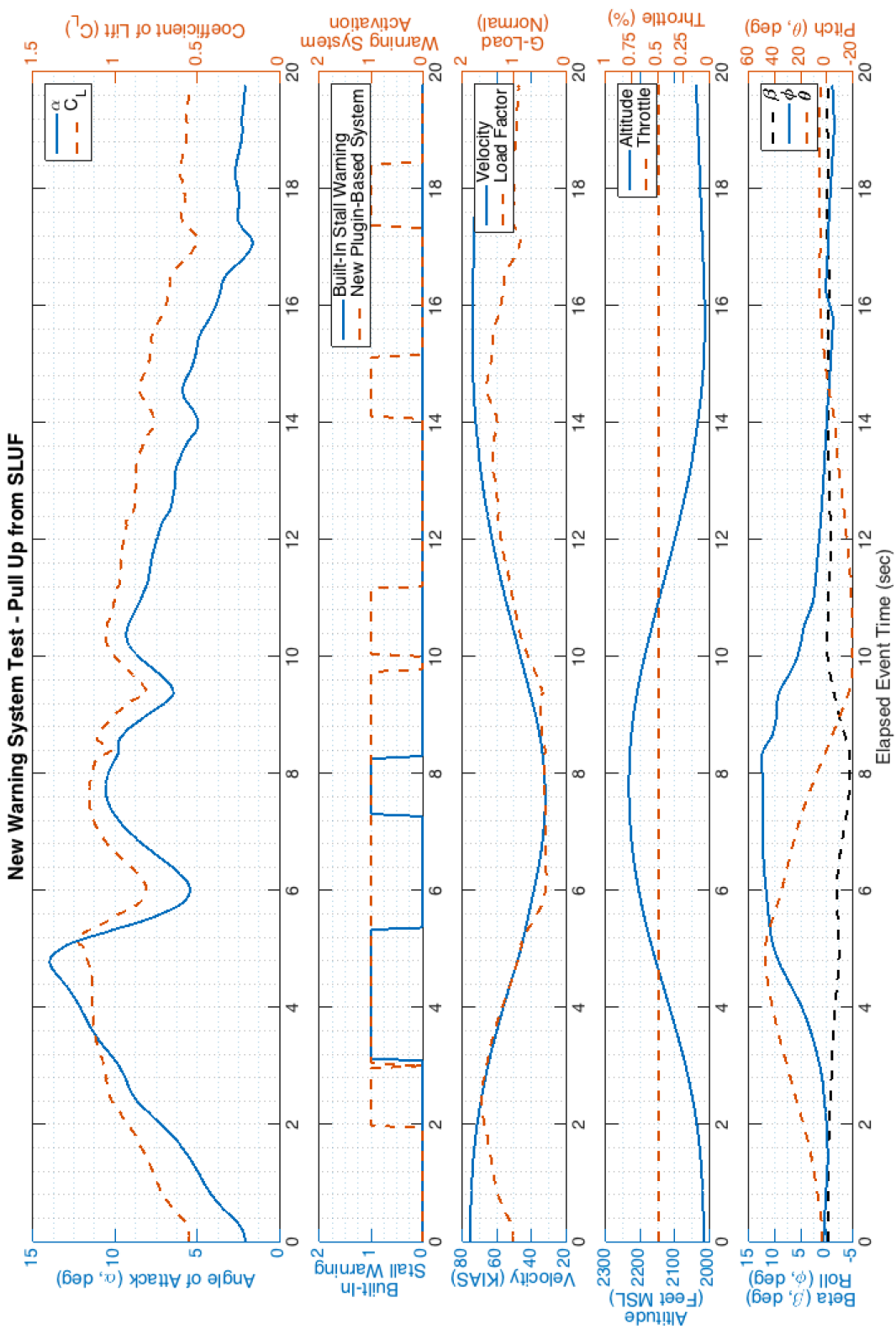

Figure C-2: Detailed time history data of fast SLUF pull up warning test

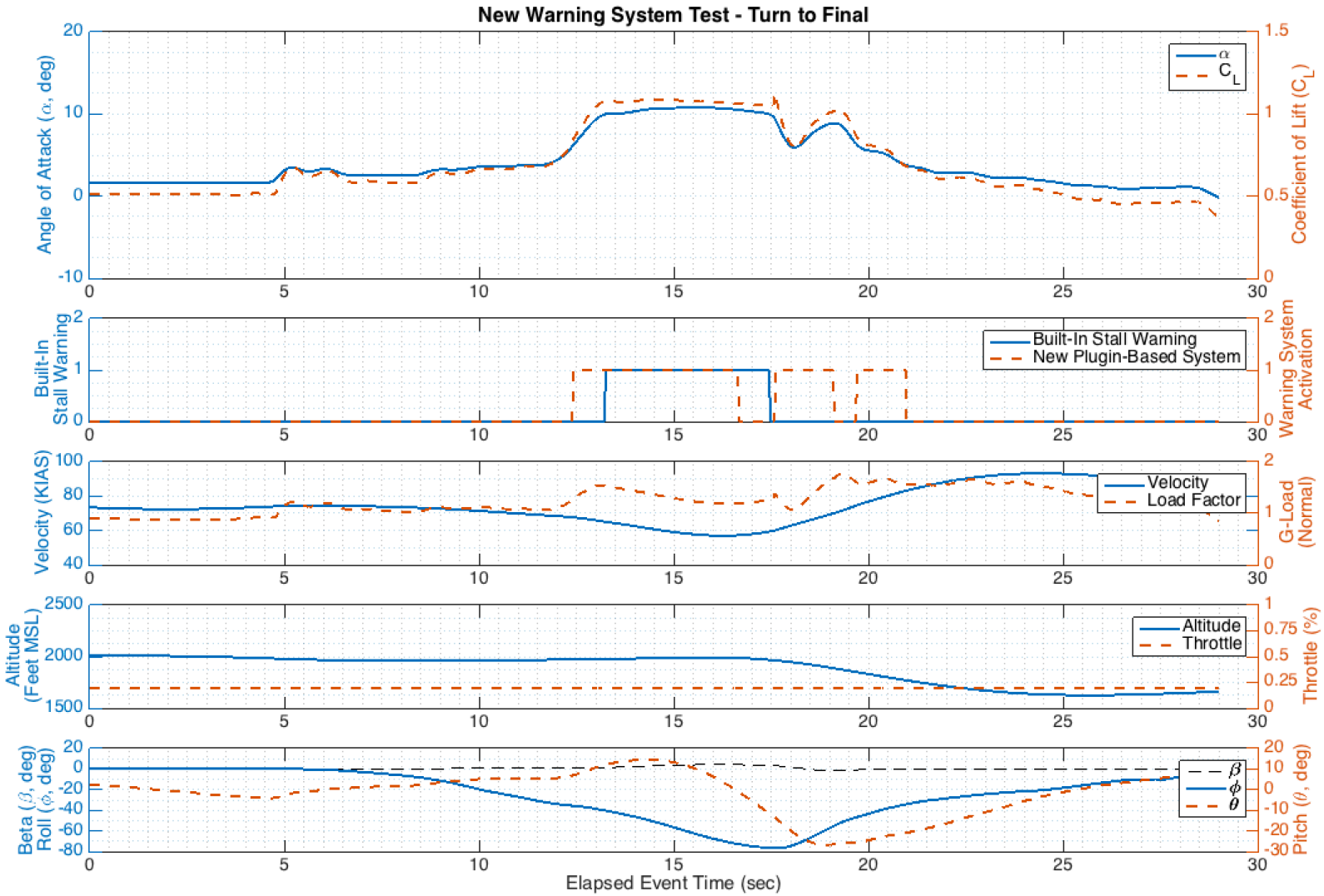

Figure C-3: Detailed time history data of "Turn to Final" warning test